A Scheme for Generating Initial Velocity Field for DNS of Isotropic Turbulence*

A. Juneja
Mason Laboratory, Yale University, New Haven, CT 06520-8286

G. Erlebacher
ICASE, NASA Langley Research Center, Hampton VA 23681-0001

K. R. Sreenivasan
Mason Laboratory, Yale University, New Haven, CT 06520-8286

Abstract

An issue to be faced in Direct Numerical Simulation (DNS) of turbulent flows is the specification of the initial velocity field which resembles closely the higher order statistics of experimentally observed turbulent flows. In this article, we report an attempt to generate a divergence-free artificial velocity field in three dimensions using ideas from the one-dimensional synthetic turbulence model [1]. A straightforward extension of the one-dimensional model proves to be computationally expensive, but we propose a simplified version whose application to the DNS of incompressible isotropic turbulence yields encouraging results. Compared to random initial conditions, the proposed scheme leads to a faster convergence of the derivative flatness and skewness of the computed velocity field and the total vorticity exhibits a monotonic decay with time. The simulations were performed on a 64^3 and a 96^3 grid using standard DNS codes.

---

* This work was supported by a grant from AFOSR, while the first author was in residence at ICASE.

1 Introduction

Over the last couple of decades, Direct Numerical Simulations (DNS) of the complete Navier-Stokes equations have emerged as a leading tool for turbulence research [2, 3]. While the current constraints on computational speed and available memory have limited the use of DNS to low Reynolds number and simple flow configurations, the importance of DNS lies in its ability to provide new insights to turbulence physics and guidance in turbulence modeling and control. Consequently simulations of isotropic turbulence form an important part of the current DNS work. In this case, the homogeneity of the flow field allows the use of periodic boundary conditions, provided care is taken to ensure that the domain is large enough to contain all unstable Fourier modes. However the specification of an initial velocity field which resembles experimentally observed turbulent flows remains an important challenge.

The current schemes for initializing the flow conditions commonly employ a random field which satisfies the continuity equation. Although this random field can be defined with a desired energy spectra and prescribed root mean square (rms) velocity fluctuations, the higher order statistics of the flow field take some time to converge as the simulation progresses and become physically realistic only after an initial period of adjustment. A related problem is that the total vorticity of the data field increases initially to a maximum value before starting to decay. This not only results in a loss of computational time but also in the decrease of the microscale Reynolds number (R_λ) of the flow at which meaningful results can be extracted from the simulation. Further, in the particular case of isotropic turbulence, the decay history is to a large degree set by the initial flow state. Hence there is the need for a technique to generate artificial vector fields which can resemble experimental data including high order statistics of velocity fluctuations.

Recently a scheme for generating artificial velocity signals, which are statistically similar to velocity fluctuations in high-Reynolds-number atmospheric flows, has been suggested in Ref. [1]. The technique generated a stochastic field dubbed as synthetic turbulence. In Ref. [1], the technique was implemented in one dimension. It consists of the following three ingredients: first, a simple multiplicative procedure is utilized for generating an intermittent signal which has the same properties as those of the turbulent energy dissipation rate, ϵ. Second, the properties of the intermittent signal averaged over an interval of size r are related to those of longitudinal velocity increments $\Delta u(r)$, evaluated over the same distance r, through a stochastic variable V introduced in the spirit of Kolmogorov's refined similarity hypothesis [4]. The third and final step consists of suitably combining velocity increments at various

scales to construct an artificial velocity signal. Several properties of the synthetic turbulence signal, obtained both analytically and numerically, were found to be in good agreement with velocity measurements made in the atmospheric surface layer. In this report, we propose an extension of the above scheme to generate a vector field in three dimensions which satisfies the incompressibility condition and can be used as the initial condition for DNS of isotropic turbulence.

The rest of the paper is organized as follows. In section 2, as a background, we provide a brief description of the synthetic turbulence technique to generate one dimensional traces of artificial velocity signals. The extension of this scheme to form a divergence-free vector field in three dimensions is discussed in Section 3. It is pointed out that a simple extension of the one-dimensional synthetic turbulence model is not computationally efficient necessitating a simplified version of the synthetic turbulence scheme. While an artificial velocity field generated using the simplified scheme has some deficiencies, a DNS of isotropic turbulence, with this field as its initial condition, yields encouraging results as shown in Section 4. The DNS scheme employed was developed at ICASE by Erlebacher et al. [5, 6]. The simulations are performed on a 64^3 and a 96^3 grid and are intended to reproduce the experimental data of Comte-Bellot and Corrsin [7]. Finally, Section 5 contains a few concluding remarks about the present scheme and scope for future work.

2 Background: One-Dimensional Synthetic Turbulence

A number of models have been proposed in recent literature [1, 8, 9, 10, 11] for constructing signals which share some properties of turbulent velocity fluctuations. Of these, only [1] and [9] reproduce the correct skewness of velocity increments and the scaling of odd-order structure functions. In this section, we present a brief description of one of the above schemes, the synthetic turbulence model [1], for generating one-dimensional traces which do not differ significantly from velocity fluctuations in real turbulence in the sense of one-point and two-point statistics.

As mentioned before, implementation of the one-dimensional synthetic turbulence model requires the following three steps:

(a) A multiplicative procedure is utilized for generating an intermittent positive signal (or measure) possessing many of the properties of turbulent energy dissipation, ϵ. Construction of this measure by one of the possible multiplicative procedures,

the p model [12], is shown schematically in Fig. 1. (The measure so generated will be denoted by the symbol d later in the text.)

(b) The properties of the measure contained in a box of size r are related to those of velocity increments $\Delta u(r)$ over the same separation distance r. This is done *via* a stochastic variable V introduced in the spirit of Kolmogorov's refined similarity hypotheses [4], which relate the probability distribution function (pdf) of velocity increment $\Delta u(r) = u(x+r) - u(x)$ to the dissipation rate in the segment $[x, x+r]$, namely $r\epsilon_r(x)$. Defining a velocity scale at location x by $U_r = (r\epsilon_r)^{1/3}$ and a local Reynolds number $Re_r = rU_r/\nu$, the refined similarity hypotheses state that for $r \ll L$ (L being the integral scale of turbulence)

$$\Delta u(r) = V(r\epsilon_r)^{1/3}, \tag{1}$$

where V is a stochastic variable with a universal form for the pdf when $Re_r \gg 1$. (See Ref. [13] for a recent work relating to the statement of the hypotheses.) By choosing the stochastic variable V randomly from a Gaussian distribution[1] the properties of the p model measure can be related to a velocity increment like quantity following Eq. (1).

(c) The third and final step consists of constructing the artificial velocity signal by suitably combining the velocity increments at different scales. By using a technique similar to the midpoint displacement method [15] for generating traces of fractional Brownian motion [16] (shown in Fig. 2), the velocity increments are represented as the amplitude of skewed tent functions (Fig. 3), and the artificial velocity signal is a superposition of a large number of these tent functions of varying scales and locations.

The composite model for generating the artificial velocity signal on a unit interval can be written as:

$$u(x) = U_0 \sum_{m=1}^{N} \left[V_m \left(\sum_{i=\beta_m}^{\beta_m + 2^{-\alpha_m}} d_i \right)^{1/3} \right] T^{(V_m)} \left(2^{-\alpha_m} (x - \beta_m) \right). \tag{2}$$

Here d_i represents the p model intermittent measure; $r = 2^{-\alpha_m}$ is the scale of the velocity increment, with α chosen randomly from the following distribution:

$$P(\alpha) = \frac{\ln 2 \; 2^{\alpha}}{2^{\alpha_{max}} - 2^{\alpha_{min}}}, \qquad \alpha_{min} < \alpha < \alpha_{max} \; , \tag{3}$$

[1]The pdf of V computed from experimental data [13] is found to be close to a Gaussian (with variance $\sim$ 2), but not exactly so; consistency with Kolmogorov's $4/5th$ law [14] demands $\langle V^3 \rangle$ = -0.8. Hence the pdf has a small skewness of about -0.3.

α_{min} and α_{max} corresponding to the largest and the smallest scale respectively; the location β_m is chosen randomly from a uniform distribution on the unit interval; and the quantity U_0 provides the velocity units for the tent functions which are defined as follows:

$$T^{(+)}(\mu) = \begin{cases} \mu/s & \text{if } 0 < \mu < s \\ (1-\mu)/(1-s) & \text{if } s < \mu < 1 \\ 0 & \text{otherwise} \end{cases} \tag{4}$$

and

$$T^{(-)}(\mu) = \begin{cases} \mu/(1-s) & \text{if } 0 < \mu < 1-s \\ (1-\mu)/s & \text{if } 1-s < \mu < 1 \\ 0 & \text{otherwise.} \end{cases} \tag{5}$$

Here, s is the skew parameter[2] and is equal to 0.88 for the synthetic turbulence signal to be consistent with Kolmogorov's $4/5th$ law [14]. The dependence of $T^{(V_m)}$ (the superscript (V_m) referring to the sign of the amplitude) on the sign of V_m is necessary in order to preserve the space reversal symmetry of the Navier-Stokes equations. Also, the continuous distribution for the scales and locations satisfies the continuous scale symmetry imposed by the Navier-Stokes equations.

The expression for $u(x)$ (Eq. (2)) has an alternative interpretation as terms of a wavelet expansion whose coefficients are related to the velocity increments at different scales, with the number N (of the tents being superposed) exactly corresponding to the coefficient count in such a basis. However, both α and β are chosen from a continuous distribution unlike a dyadic hierarchy of scales of elements in a wavelet expansion, but the distribution of scales (Eq. (3)) constitutes a generalization to the continuous case of a wavelet-basis description of the signal.

All the parameters of the synthetic turbulence signal are shown to be related to those of real turbulence in [1]. Specifically, relations can be established between the size of the largest tent function $r = 2^{-\alpha_{min}}$, and the integral length scale L; the size of the smallest tent function $r = 2^{-\alpha_{max}}$, and the Kolmogorov length scale η; U_0 and root mean square (rms) velocity fluctuations u_{rms}; s and the skewness of velocity increments, p (p model multiplier) and the structure function scaling exponent [3] ζ_n for some n. The properties of the synthetic turbulence model, computed both analytically and numerically, show excellent agreement with those of velocity fluctuations in the atmospheric surface layer. Among the properties of the artificial

[2]Setting s = 0.5 will yield a zero value for the skewness of the velocity increments.

[3]The structure functions can be defined as $\langle \Delta u_r^n \rangle = \langle (u(x+r) - u(x))^n \rangle \sim r^{\zeta_n}$, where n is the order of the structure function and ζ_n is the corresponding structure function exponent.

velocity signal examined in [1] are its power spectrum, the scaling of odd and even order structure functions up to the $8th$ order, Kolmogorov's refined similarity hypotheses, its fractal dimension, derivative skewness as well as the multifractal scaling of ϵ_r constructed from synthetic turbulence signal.

The success of the one-dimensional synthetic turbulence model in duplicating the statistical properties of experimentally observed velocity fluctuations in turbulent flows suggests that the physical elements which go into the construction are good abstractions of the reality, and further that the statistical ordering in turbulence can be approximated relatively simply for most practical purposes. However, in order for a model to be useful for work with simulations, we need to generate the complete velocity field in three dimensions. This is attempted in the next section.

3 Artificial Velocity Field in 3-dimensions

We begin this section by outlining the changes that need to be implemented for a simple extension of the one-dimensional synthetic turbulence model to generate a divergence-free vector field in three dimensions. Such a model however requires an inordinate amount of computer time for grids which are 128^3 points or larger. Hence we propose a simplified model which employs a hierarchical (instead of random) construction scheme for the artificial velocity field. While this artificial velocity field does not duplicate all the properties of velocity fluctuations in real turbulence, it will be seen in the next section that a DNS of isotropic turbulence which uses this field as its initial condition yields encouraging results.

The simplest extension of one-dimensional synthetic turbulence to generate a single component of velocity in three dimensions involves the following changes. First, a three-dimensional version of the p model is employed to generate an intermittent measure resembling turbulent energy dissipation. Briefly, the three-dimensional p model builds up an intermittent measure by dividing a cube of linear size r into eight smaller cubes of linear size $r/2$ such that half of the smaller cubes (randomly assigned) share a fraction p of the parent measure, while the other half share a fraction $1-p$ of the parent measure. Similar to the one-dimensional case, the value of $p = 0.7$ yields a measure (denoted by $d_{i,j,k}$ later in the text) whose statistical properties are similar to those of turbulent energy dissipation. Hence, at any scale r and location $\vec{\beta} = (\beta_i, \beta_j, \beta_k)$, the quantity analogous to $r\epsilon_r$ in real turbulence can

be expressed as

$$D_{\vec{\beta}} = \frac{1}{r^2} \sum_{i=\beta_i}^{\beta_i+r} \sum_{j=\beta_j}^{\beta_j+r} \sum_{k=\beta_k}^{\beta_k+r} d_{i,j,k} \tag{6}$$

The properties of $D_{\vec{\beta}}$ can then be related to velocity increments across a scale r, *via* the stochastic variable V in the spirit of Kolmogorov's refined hypotheses (Eq. (1)) as before. The final modification of the one-dimensional model involves the definition of tent functions (whose amplitude represent the appropriate velocity increment) which are now modified to have a three-dimensional support in the following manner:

$$T_{3D}^{(+/-)}(a,b,c) = T^{(+/-)}(a) \times T^{(+/-)}(b) \times T^{(+/-)}(c) \tag{7}$$

for $0 < a < 1$, $0 < b < 1$, and $0 < c < 1$. Here the function $T^{(+/-)}$ is the same as one defined in Eqs. (4) and (5). A scalar field in three dimensions can then be formed by a superposition of a large number of these tents of varying amplitudes, scales and locations. The composite model for generating the scalar field on a unit cube can be expressed in a form similar to Eq. (2) except that in this case $\mathbf{x}$ and $\vec{\beta}$ are vectors.

$$u(\mathbf{x}) = U_0 \sum_{m=1}^{N} \left[V_m \left(D_{\vec{\beta}_m} \right)^{1/3} \right] T_{3D}^{(V_m)} \left(2^{-\alpha_m} (\mathbf{x} - \vec{\beta}_m) \right) . \tag{8}$$

Here $r = 2^{-\alpha_m}$ represents the linear size of the three-dimensional support for the tent function; the α's being picked from the same distribution as before (Eq. (3)). Each of the three components of $\vec{\beta}$ are chosen from a uniform distribution on the unit interval and the quantity $D_{\vec{\beta}_m}$ is computed using Eq. (6). The number N of the tent functions being superposed corresponds to the number of coefficients in a three-dimensional wavelet-basis expansion.

In order to generate a divergence-free vector field, one further detail is necessary. First, the scheme outlined by Eq. (8) is used to generate three independent scalar fields u', v' and w', which together define the vector field $\mathbf{u^F} = (u', v', w')$. Next, $\mathbf{u^F}$ can be decomposed into the sum

$$\mathbf{u^F}(\mathbf{x}) = \mathbf{u}(\mathbf{x}) + \mathbf{u^C}(\mathbf{x}) \tag{9}$$

where

$$\nabla \cdot \mathbf{u} = 0 \, , \qquad \nabla \times \mathbf{u^C} = 0 \, . \tag{10}$$

This decomposition is unique and can be accomplished in Fourier space according to the prescription

$$\hat{\mathbf{u}} = \hat{\mathbf{u}}^{\mathbf{F}} - \frac{\mathbf{k} \cdot \hat{\mathbf{u}}}{k^2} \mathbf{k} , \qquad \hat{\mathbf{u}}^{\mathbf{C}} = \hat{\mathbf{u}}^{\mathbf{F}} - \hat{\mathbf{u}} . \tag{11}$$

The final divergence-free vector field in three dimensions can then be formed by transforming $\hat{\mathbf{u}}$ back to physical space.

We generated a vector field using the above scheme on a 64^3 grid. Figure 4(a) shows a plot of the pdf of the three components of $\mathbf{u}$, while Fig. 4(b) shows a one-dimensional power spectrum of one component of the velocity. Figure 5 shows the scaling of the second, third and fourth order structure functions. As can be observed, there is not much of a scaling regime in the plot due to very small inertial range. However, to a rough approximation, the scaling exponents seem to be in agreement with experimental results. In order to document the fact that taking the solenoidal projection to define the divergence-free velocity field does not appreciably alter the scaling properties of the velocity field, we present in Figs. (6)-(8), the PDF of individual velocity components, three-dimensional energy spectra of the velocity field, and the longitudinal structure functions before and after the solenoidal projection.

A major drawback of such a straightforward extension of the one-dimensional model is that it is not computationally efficient. The amount of CPU time required to generate the divergence-free vector fields ranges from 140 seconds on a 64^3 grid to about 6000 seconds on a 128^3 grid. This renders the three-dimensional synthetic turbulence model to be essentially useless for DNS work. So simplifications to the above scheme are necessary. Part of the computational complexity of the three-dimensional synthetic turbulence model arises from the random locations and scales of the tent functions while some of it stems from the requirement of periodic boundary conditions at the domain boundaries (by this we mean that if a part of tent function overshoots the domain boundary then it is placed beginning from the opposite face of the domain). Hence a possible simplification to the synthetic turbulence scheme involves utilization of a hierarchical construction process without enforcing periodic boundary condition. One such simplification of the synthetic turbulence model is discussed below.

In this instance, we start by considering a cube of linear size L on which a measure is defined to be uniform; the total value of the measure equals ($L^3\langle\epsilon\rangle$). (This is analogous to the zero-th step in the three-dimensional p-model construction.) The information about the total value of the measure in the cube is then used to

determine the quantity $L\langle\epsilon\rangle$. Following Eq. (1), the quantity $L\langle\epsilon\rangle$, is converted into a velocity increment across the scale L using a stochastic variable V picked from a Gaussian distribution. Next, this velocity increment is represented as the amplitude of a three-dimensional tent function (defined by Eq. (7)) whose scale and location correspond to that of the cube itself. In the second step of the construction, the cube of size L is divided into eight non-overlapping equal parts (cubes of linear size $L/2$), while the measure itself is divided such that half of the smaller cubes (chosen randomly) share a fraction 0.7 of the parent measure while the remaining cubes share a fraction 0.3 of the parent measure. The information about the total measure in each of the eight smaller cubes is again related to velocity increments across a scale $L/2$. These velocity increments are next represented as the amplitude of the 3-d tent functions whose scale and location correspond exactly to those of the eight smaller cubes. This process is repeated for n number of steps, at the end of which a scalar field in three dimensions can be generated by a superposition of the 3-d tent functions defined at each stage of the construction process. Note that this scheme can be expressed in exactly the same form as Eq. (8), except that the scales and locations are no longer determined from a continuous distribution. Also the quantity $D_{\vec{\beta}_m}$ is now simply $\frac{1}{r^2}$ of the total measure contained in the cube (of linear size r) of interest. Once again a vector field $\mathbf{u^F}$ can be defined by generating three independent scalar fields (u', v', and w') using the simplified scheme. We can then define a divergence-free artificial velocity field by taking the solenoidal projection of the complete vector field following Eqs. (9), (10) and (11).

A look at the statistical properties of the artificial velocity field generated using the simplified scheme on a 64^3 grid reveals some differences from those obtained using the complete synthetic turbulence model. Firstly, the power spectrum of the artificial velocity exhibits spikes (although the background has the right slope), indicating a lack of continuous scale symmetry. The reason for this is that during the construction process a cube is rigidly divided into eight equal parts at each step, which imposes a fixed grid on to the field. However this is not a serious problem, and can be overcome by artificially removing the spikes in Fourier space without affecting any of the other statistical properties. Alternatively, one can use the untampered field as the initial condition; it can be readily seen that the first few time steps of the simulation quickly smear out these spikes. The second and more serious problem relates to the convergence of statistics and arises due to the small grid size of the computational domain which limits the number of steps in the construction process to a maximum of just four. Also since the tent functions are no

longer located randomly in the domain with periodic boundary conditions, the large fraction of points near the boundary to the total number of points in the domain for a small grid size, result in the velocity being close to zero at many points in the domain. To alleviate this problem, a further modification in the simplified technique is necessary. Instead of defining a single component (u', v', or w') of the vector field $\mathbf{u^F}$ to be one realization of the simplified model, we shall superpose a number of these realizations (between 10 and 20) to form u', v' and w' [4]. This superposition can be achieved by either placing the realizations atop one another, or by locating them randomly in the computational domain and wrapping them around (similar to imposing periodic boundary conditions). It is observed that the first approach (of placing realizations atop one another) leads to a better convergence to correct values of higher-order statistics. In Fig. 9(a) we show a plot of the pdf of the three components of the artificial velocity field. In this case, u', v' and w' were formed by a superposition of twelve realizations of the simplified scheme atop one another. Fig. 9(b) shows the power spectrum density of a single component of the final velocity field. As mentioned before, the power spectrum has spikes because of the imposed grid in the generation scheme. The observed scaling of the second and fourth order structure function (plotted in Fig. 10) using the simplified technique is as good as that for the complete synthetic turbulence model (Fig. 5). However the scaling of the third order structure function is not as good and this problem is related to the poor convergence properties of the velocity field using the simplified scheme. One last observation in this regard is that if one generates a field with non-skewed velocity increments, some fourth order statistics (for example the derivative flatness) converge faster to the correct value compared to the case when the artificial velocity field has the correct skewness for velocity increments.

To summarize, the best compromise for generating a divergence-free vector field in a reasonable amount of computer time, employs a hierarchical construction scheme to generate one realization of a scalar field. Several realizations of the scalar field thus formed are superposed to yield a single component of the vector field $\mathbf{u^F}$. Finally, by taking a solenoidal projection of $\mathbf{u^F}$, one can define an artificial velocity field $\mathbf{u}$, in three dimensions which satisfies the incompressibility condition. In the next section, we will use this velocity field as the initial condition for DNS of decaying isotropic turbulence.

[4] This is in some sense equivalent to extracting statistics from the field by averaging over a number of largest eddies, since in each case the size of largest eddy is equal to the size of the domain itself

4 Results from DNS

The simulations presented in this section are performed using the DNS code for compressible turbulent flows developed at ICASE by Erlebacher and colleagues. This code can be used for simulations of incompressible flows by a judicious choice of the input parameters and this will be discussed later. The DNS code was run with the simplified synthetic turbulence initial conditions as well as random initial conditions to match the experimental observations of Comte-Bellot and Corrsin [7] on isotropic turbulence. The results from these simulations are summarized at the end of the section.

We shall provide only a brief outline of the numerical scheme here and refer the reader to [5, 6] for more details. The compressible turbulent flow of an ideal gas is governed by the continuity, momentum and energy equations (see, for example, Ref. [17] for complete equations). These equations are first expressed in a non-dimensional form, with the time derivative in the energy equation written solely in terms of pressures. Next, in order to alleviate the severe stability requirements imposed at very low Mach numbers by acoustic waves, a splitting method is adopted, with the second fractional step containing most of the effects of the acoustic waves. The spatial derivatives in the first fractional step of the equations are approximated by a Fourier collocation method (see for example Ref. [18]). The second fractional step is integrated analytically in Fourier space so it does not contribute to time step limitations. The numerical anisotropy is reduced by performing an isotropic truncation during the acoustic fractional step by setting all Fourier coefficients for which $k_l k_l \geq (N/2)^2$ equal to zero for each variable (ρ, $\rho\mathbf{u}$ and p).

The input parameters of interest are the reference Mach number, initial ratio of compressible to solenoidal energy, initial value of root mean square (rms) density fluctuations, velocity fluctuations, temperature fluctuations and mach number fluctuations. By using a very low value of the reference Mach number (~ 0.05) and setting the initial rms density fluctuations and the ratio of compressible to solenoidal energy to be zero, one can use the DNS code for simulations of incompressible flows. Care is taken to ensure that the divergence of the velocity field remains close to zero, as also the ratio of the compressible to solenoidal energy during any step of the simulation.

In order to compare their relative merits, we generated two artificial velocity fields using the simplified technique. In the first instance, the derivative skewness of the velocity field was set close to zero, leading to a better convergence for the value of the derivative flatness. The second artificial velocity field had the correct

value of the derivative skewness but the derivative flatness was a little higher than its equilibrium value. Both these velocity fields were used as the initial condition for a DNS of incompressible isotropic turbulence. For purposes of comparison, a DNS with random initial conditions was also performed. The simulations were intended to reproduce the experimental data of Comte-Bellot and Corrsin [7] on isotropic turbulence, hereafter referred to as CBC. The computational domain is a cube of size $20/2\pi$ cm. The reference length (L_0), velocity (U_0) and pressure (P_0) are respectively $20/2\pi$ cm, 1 cm/sec, and 1 $gr/cm\text{-}sec^2$. The kinetic energy of the initial velocity field was scaled to match the measured CBC energy spectrum at a non-dimensional time of 240. With the chosen non-dimensionalization, the Reynolds number $Re = U_0 L_0/\nu$ is 22.74 based on a kinematic viscosity $\nu = 0.14$ cm^2/sec. Table 1 summarizes the parameters of the initial conditions and the corresponding CBC observations.

	CBC	*Rand*-64	*Skew*-64	*Flat*-64	*Flat*-96
$\mathbf{v}_{rms}$	6.75	6.75	6.75	6.75	6.75
E	-	68.3	68.3	68.3	68.3
ϵ	462	374	364	369	428
$\frac{1}{3}tr(\mathbf{Sk})$	-	-0.01	-0.26	-0.03	-0.03
$\frac{1}{3}tr(\mathbf{Fl})$	-	3.0	4.5	3.75	4.8
λ_{11}	0.26	0.28	0.35	0.30	0.26
λ_{22}	-	0.20	0.20	0.20	0.17
λ_{33}	-	0.19	0.19	0.20	0.17
$R_{\lambda_{11}}$	38.1	42.6	53.1	46.1	42.5

Table 1: Summary of the Initial Conditions for the DNS run based on the CBC experiment

The columns in Table 1 correspond to experimental measurements of Comte-Bellot and Corrsin at t = 240 in their units (CBC) (cf. Table 4 in [7]), random initial conditions on a 64^3 grid (*Rand*-64), simplified synthetic turbulence initial conditions with correct derivative skewness on a 64^3 grid (*Skew*-64), simplified synthetic turbulence initial conditions with zero derivative skewness on a 64^3 grid (*Flat*-64), and simplified synthetic turbulence initial condition with zero derivative skewness on a

96^3 grid (*Flat*-96). In the table, the Taylor microscale length λ_{kl} is defined by

$$\lambda_{kl} = \left[\frac{\langle v_k^2 \rangle}{\left\langle \left(\frac{\partial v_k}{\partial x_l} \right)^2 \right\rangle} \right]^{1/2} \tag{12}$$

and the dissipation ϵ by

$$\epsilon = 2\mu \int S_{ij} S_{ij} d^3x, \tag{13}$$

where S_{ij} is the stress tensor

$$S_{ij} = \frac{1}{2} \left(\frac{\partial v_i}{\partial x_j} + \frac{\partial v_j}{\partial x_i} \right). \tag{14}$$

The Taylor microscale Reynolds number is

$$R_{\lambda_{11}} = \frac{v_1 \lambda_{11}}{\nu}. \tag{15}$$

The velocity derivative skewness and Flatness tensors **Sk** and **Fl** are the third and fourth moments of the velocity gradient and are defined by

$$Sk_{ij} = \frac{\left\langle \left(\frac{\partial v_i}{\partial x_j} \right)^3 \right\rangle}{\left\langle \left(\frac{\partial v_i}{\partial x_j} \right)^2 \right\rangle^{3/2}} \tag{16}$$

$$Fl_{ij} = \frac{\left\langle \left(\frac{\partial v_i}{\partial x_j} \right)^4 \right\rangle}{\left\langle \left(\frac{\partial v_i}{\partial x_j} \right)^2 \right\rangle^2}. \tag{17}$$

We can observe from Table 1 that there is some discrepancy between the experimentally observed dissipation and that computed from initial conditions. This is especially true on the smaller grid, suggesting a 64^3 grid has a marginal resolution, at best. Table 2 provides a comparison of the experimentally measured parameters with those from the numerical simulations at a nondimensional time $t = 0.11$ (in our units) which corresponds to $t = 375$ (in CBC units).

Figures 8 through 11 summarize the time evolution of some properties from the simulation performed on the 96^3 grid with *Flat*-96 initial conditions. These plots

are representative of all the three simulations which employed simplified synthetic turbulence initial conditions (*Skew*-64, *Flat*-64 and *Flat*-96). Figure 11(a) shows the spectral density of the initial velocity field ($t = 0$) while Fig. 11(b) shows the spectral density of the velocity field at a nondimensional time $t = 0.11$. The decay of total energy and dissipation with time is plotted in Fig. 12. Figure 13 plots the time evolution of λ_{3d} (3-D Taylor microscale) and $R_{\lambda_{3d}}$ (Reynolds number based on $\lambda_3 d$). Figure 14(a) shows a plot of the integral of squared vorticity as a function of time, while Fig. 14(b) plots the integral of divergence of velocity squared as a function of time. The last plot provides some confirmation about the success of the DNS code for quasi-incompressible flows. This was also checked by computing the ratio of the compressible to solenoidal energy (which remained constant near zero) and the Mach number of the flow (which decayed slightly from 0.05). Another quantity of interest is the evolution of $\langle\epsilon\rangle L/u^3$ with time. Figure 15 shows a plot of $\langle\epsilon\rangle L/u^3$ as a function of the microscale Reynolds number and this is in good agreement with Figure xx of Sreenivasan [19] which plots data from experimental measurements.

Next, we take a closer look at the time evolution of the trace of derivative skewness and flatness tensors computed from the velocity fields from simulations using all four of the initial conditions mentioned above. Figure 16(a) shows a comparison of the trace of derivative skewness from a DNS employing random initial conditions (*Rand*-64) and a DNS employing *Flat*-64 initial conditions (artificial velocity field generated from simplified synthetic turbulence model with non-skewed velocity increments). The derivative skewness is observed to equilibriate similarly fast in both cases. However the trace of the derivative flatness tensor (Fig. 16(b)) shows better convergence properties for the DNS employing *Flat*-64 initial conditions compared to random initial conditions. In the first case, the trace of the derivative flatness quickly settles down around the initial value of 3.8, while in the second case (using *Rand*-64 initial condition), it displays a slow monotonic rise from an initial value of 3.0. The DNS using *Flat*-64 initial conditions was carried out for a longer period of time to confirm the convergence values of derivative skewness and flatness deduced from Fig. 16 and the results are shown in Fig. 17. It is observed that the trace of derivative flatness stays around 3.8, while that of derivative skewness remains around -0.3. On the other hand, using an artificial velocity field from the simplified synthetic turbulence model with a correct value of skewness of velocity increments (*Skew*-64) does not do any better than random initial conditions, as shown in Fig. 18 - while the derivative skewness first oscillates before settling down, the derivative flatness exhibits a slow decay from an initial value of 4.5. Figure 19 presents the results from a DNS on a 96^3 grid using *Flat*-96 initial conditions (artificial velocity

field generated from simplified synthetic turbulence model with non-skewed velocity increments) It is observed that the derivative flatness quickly settles down near its initial value. For purposes of comparison we reproduce in Fig. 20 a plot from Ref. [6] (Fig. (6)) where the derivative flatness seems to be still evolving at the end of the simulation. Here, the DNS was carried out on a 96^3 grid using random initial conditions which were scaled to match the observed CBC spectrum.

We summarize our findings in Tables 3 and 4, which present information related to the amount of CPU time required to generate Simplified Synthetic Turbulence (SST) initial conditions and the number of iterations required to get converged values of derivative skewness using different initial conditions.

The results presented in this section indicate that a DNS employing simplified synthetic turbulence initial conditions (with non-skewed velocity increments) yields better results than a DNS employing random initial conditions, in terms of the decay of total vorticity and the convergence of derivative flatness and skewness. The simulations also underline the importance of specifying an initial velocity field having the correct initial value of the derivative flatness since it takes much longer to converge otherwise. On the other hand - no matter what the starting value - the derivative skewness equilibriates quickly to its correct value.

5 Conclusions

We report on an attempt to generate an artificial velocity field in three dimensions, which can be employed as initial condition for DNS work, using ideas from the one-dimensional synthetic turbulence model. It is observed that a straightforward extension of the one-dimensional scheme to generate a velocity field in three dimensions is computationally inefficient in order for it to be useful. Consequently we outline a simplified version of the model which compromises the convergence properties of certain higher-order statistics. A DNS employing the artificial velocity field (generated using the simplified scheme with non-skewed increments) as its initial condition leads to a much faster equilibriation of statistics of the computed velocity field compared to using random initial conditions. Presently, we would not like to place much emphasis on the success of the scheme, because the real validation will come only when the scheme is used for DNS in larger computational domains (256^3 or 512^3). Moreover, there is room for improvement in the simplified model to yield better convergence of higher order statistics. Finally, a model which builds in the correct dissipation-range properties alongwith the inertial range properties, may

prove to better for work with simulations.

The importance of developing a good model to generate an artificial velocity fields resembling turbulence is not limited to its use as initial condition for DNS work. Another application of such a model lies in its ability to provide inflow conditions for studying the decay of isotropic turbulence using DNS, by using planar slices from a single realization of the artificial velocity field in three dimensions. Further, the ingredients used to construct artificial velocity fields also allow us to obtain an expression for an effective viscosity needed to define a subgrid-scale model for Large Eddy Simulations (LES). Similar models can also be developed for scalar fluctuations in isotropic turbulence as well as for velocity fields in shear flows.

References

[1] A. Juneja, D.P. Lathrop, K.R. Sreenivasan and G. Stolovitzky, Phys. Rev. E **?**, May 1994.

[2] R.S. Rogallo and P. Moin, Ann. Rev. of Fluid Mech. **8**, 99 (1984).

[3] W.C. Reynolds, in *Whither Turbulence*, 1989.

[4] A. N. Kolmogorov, J. Fluid Mech. **13**, 82 (1962).

[5] G. Erlebacher, M.Y. Hussaini, H.O. Kreiss and S. Sarkar, ICASE Report No. **90-15** 1990.

[6] G. Erlebacher, M.Y. Hussaini, C.G. Speziale and T.A. Zang, J. Fluid Mech. **?**, ? (199?).

[7] G. Comte-Bellot and S. Corrsin, J. Fluid Mech. **48**, 1971.

[8] J. A. C. Humphrey, C. A. Schuler and B. Rubinsky, Fluid. Dyn. Res. **9**, 81, (1992).

[9] J. Eggers and S. Grossmann, Phys. Rev. A **45**, 2360, (1992).

[10] T. Vicsek and A. L. Barabasi, J. Phys. A **24**, L485, (1991).

[11] R. Benzi, L. Biferale, A. Crisanti, G. Paladin, M. Vergassola, A. Vulpiani, Physica D **65**, 352, (1993).

[12] C. Meneveau and K. R. Sreenivasan, Phys. Rev. Lett., **59**, 1424 (1987).

[13] G. Stolovitzky, P. Kailasnath, and K. R. Sreenivasan, Phys. Rev. Lett. **69**, 1178 (1992).

[14] A. N. Kolmogorov, Dokl. Akad. Nauk SSSR **32**, 16 (1941).

[15] R. F. Voss, Physica D **38**, 362, (1989).

[16] B. B. Mandelbrot and J. W. Van Ness, SIAM Rev. **10**, 422 (1968).

[17] G.K. Batchelor, *An Introduction to Fluid Mechanics* (1967).

[18] M.Y. Hussaini and T.A. Zang, Ann. Rev. of Fluid Mech. **19**, 354 (1987).

[19] Sreenivasan - plot of $\epsilon L/U^3$.

Figure Captions

Fig. 1: The p-model for generating an intermittent measure $d(x)$ on a unit interval ($x \in [0,1]$), employs unequal multipliers ($p_1 = 0.7$ and $p_2 = 0.3$) to refine an initially uniform measure according to a binary scheme. The outcome of the first three steps and that at the end of nine steps are shown.

Fig. 2: Construction of fractional Brownian motion using the midpoint addition method. At each successive stage the increment across a scale τ, $\Delta X(\tau)$ (see Eq. (10) is represented by the amplitude of the tent function $T(t)$, whose base is equal in size to the scale τ. The fBm is formed by superimposing tent functions of all scales (up to some level of refinement), illustrated for the first three steps in (a), (b) and (c); (d) shows the superimposed signal $X(t)$ after 8 steps in the construction.

Fig. 3: Basic tent functions $T^{(+)}$ and $T^{(-)}$ used in the synthetic turbulence models. As $T^{(-)}$ will always appear in the construction multiplied by a negative number, we have plotted $-T^{(-)}$.

Fig. 4: (a) The probability distribution function of the three components (u, v, and w) of the artificial velocity field generated on a 64^3 grid using a straightforward extension of the 1-d synthetic turbulence model. The solid line in the plot represents a Gaussian distribution. (b) The power spectrum of a single component (u) from the artificial velocity field described above. The dashed line whose slope is roughly $-5/3$ gives an indication of the inertial range.

Fig. 5: The scaling of the second, third and fourth order structure functions for a single velocity component u in the x direction; u being the component of the same artificial velocity field as Fig. 4. The dashed lines in each of the plots represent a least squares fit in the inertial range of scales yielding $\zeta_2 = 0.69$, $\zeta_3 = 1.0$, and $\zeta_4 = 1.29$. However this should not be taken very seriously as the scaling regime is extremely limited.

Fig. 6: The probability distribution function of the three components (u, v, and w) of the artificial velocity field (a) before and (b) after taking the solenoidal projection. The solid line in the plot represents a Gaussian distribution.

Fig. 7: The three-dimensional energy spectrum of the artificial velocity before (solid

line) and after (dotted line) taking the solenoidal projection. The dashed line in the plot has a slope of approximately -1.7.

Fig. 8: The scaling of the second, third and fourth order longitudinal structure functions for different velocity components (u - solid line, v - dashed line and w - dotted line) (a) before and (b) after taking the solenoidal projection.

Fig. 9: (a) The probability distribution function of the three components (u, v, and w) of the artificial velocity field generated on a 64^3 grid using the simplified version of the complete synthetic turbulence model. The solid line in the plot represents a Gaussian distribution. (b) The power spectrum of a single component (u) from the artificial velocity field described above. The presence of spikes is due to the imposed grid in the hierarchical construction process.

Fig. 10: The scaling of the second, third and fourth order structure functions for a single velocity component u in the x direction. u being the component of the same artificial velocity field as Fig. 9. The dashed lines in each of the plots represent a least squares fit in the inertial range of scales yielding $\zeta_2 = 0.7$, $\zeta_3 = 0.95$, and $\zeta_4 = 1.23$. The scaling of the second and fourth order structure functions seem to be slightly better than Fig. 5, while that of third order structure function is not as good.

Fig. 11: (a) The 3-d energy spectrum of the initial velocity field (*Flat*-96) used for DNS of decaying isotropic turbulence on a 96^3 grid. The velocity field was generated using the simplified synthetic turbulence model (with non-skewed velocity increments) and then its energy spectrum was scaled to match the experimental observations of Comte-Bellot and Corrsin [7]. (b) The energy spectrum of the velocity field from the DNS at a non-dimensional time $t = 0.11$.

Fig. 12: The decay of (a) energy and (b) dissipation as a function of time from a DNS employing *Flat*-96 initial conditions.

Fig. 13: A plot of (a) 3-d Taylor microscale λ_{3d} and (b) Reynolds number based on λ_{3d} as a function of time from a DNS employing *Flat*-96 initial conditions.

Fig. 14: A plot of (a) integral of squared vorticity and (b) integral of squared divergence of velocity field as a function of time from a DNS employing *Flat*-96

initial conditions.

Fig. 15: The dependence of the quantity $\langle\epsilon\rangle L/u^3$ on the microscale Reynolds number. See Fig. XX in Ref. [19] for a comparison with experimental measurements.

Fig. 16: Comparison of the trace of (a) derivative skewness tensor and (b) derivative flatness tensor from simulations performed on a 64^3 grid. The dashed line represents results from a DNS with random initial conditions (*Rand*-64) while the solid line represents results from a DNS with simplified synthetic turbulence initial condition with non-skewed velocity increments (*Flat*-64). The derivative skewness equilibriates similarly fast in both cases, while the use of *Flat*-64 initial conditions lead to faster convergence of derivative flatness.

Fig. 17: A plot of the trace of (a) derivative skewness tensor and (b) derivative flatness tensor as a function of time. The results are from a DNS employing *Flat*-64 initial conditions carried out for a longer period of time to confirm the convergence values of the respective statistics.

Fig. 18: Comparison of the trace of (a) derivative skewness tensor and (b) derivative flatness tensor from simulations performed on a 64^3 grid. The dashed line represents results from a DNS with random initial conditions (*Rand*-64) while the solid line represents results from a DNS with simplified synthetic turbulence initial condition (*Skew*-64). The *Skew*-64 initial conditions do not seem to perform any better than random initial conditions.

Fig. 19: A plot of the trace of (a) derivative skewness tensor and (b) derivative flatness tensor as a function of time, from a DNS employing *Flat*-96 initial conditions. The results indicate that an artificial velocity field with the correct initial value of the derivative flatness leads to better results than a artificial velocity field with the correct initial value for derivative skewness.

Fig. 20: The trace of the derivative flatness from a DNS on a 96^3 grid employing random initial conditions. The plot is reproduced from Ref. [6].

	CBC	*Rand*-64	*Flat*-64	*Skew*-64	*Flat*-96
$\mathbf{v}_{rms}$	5.03	5.32	5.29	5.29	5.29
E	38.6	42.5	41.5	41.9	41.4
ϵ	154.4	183.8	167.2	171.5	153.7
$\frac{1}{3}tr(\mathbf{Sk})$	-	-0.30	-0.25	-0.26	-0.46
$\frac{1}{3}tr(\mathbf{Fl})$	-	3.45	3.90	4.0	4.90
λ_{11}	0.34	0.31	0.34	0.32	0.34
λ_{22}	-	0.23	0.23	0.22	0.24
λ_{33}	-	0.22	0.23	0.22	0.23
$R_{\lambda_{11}}$	36.6	38.1	39.8	36.2	39.9

Table 2: Final Conditions (t = 0.11 seconds) from the simulations as well as the CBC experiment

Box Size	CPU time (sec) to generate SST on CRAY 2
64^3	25
96^3	40
128^3	75

Table 3: CPU time required to generate similplified synthetic turbulence velocity field.

Box Size	CPU time (sec) per time step iteration on CRAY-2				Number of iterations for converged derivative flatness	
	Velocity	Pressure	Energy	Scalar	RANDOM I.C.	SST MODEL
64^3	6.3	2.5	7.4	9.2	950	200
96^3	26.5	10.5	31.5	57.5	1600	330

Table 4: CPU time required on a CRAY-2 for different subroutines of the DNS code for each itretation, and the number of iterations required to get convergent value of the derivative skewness using different initial conditions.

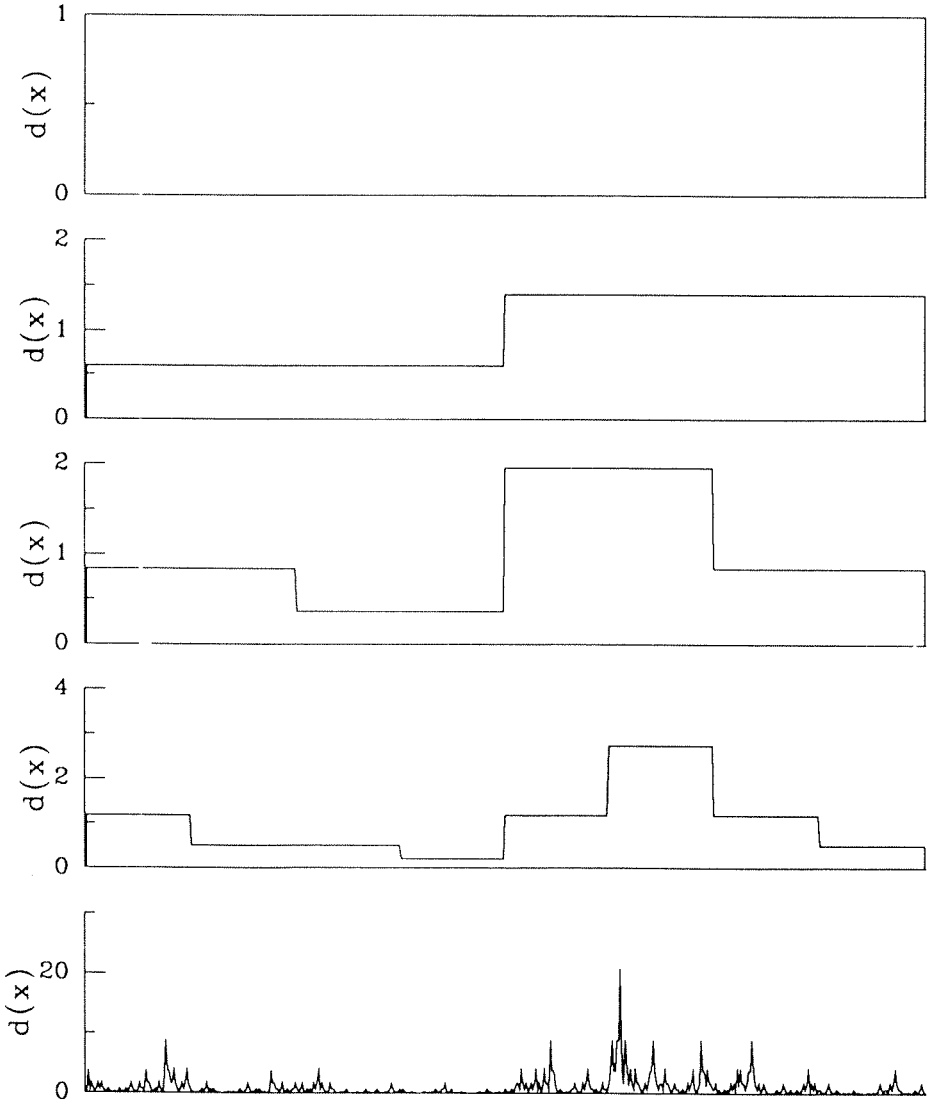

FIG 1

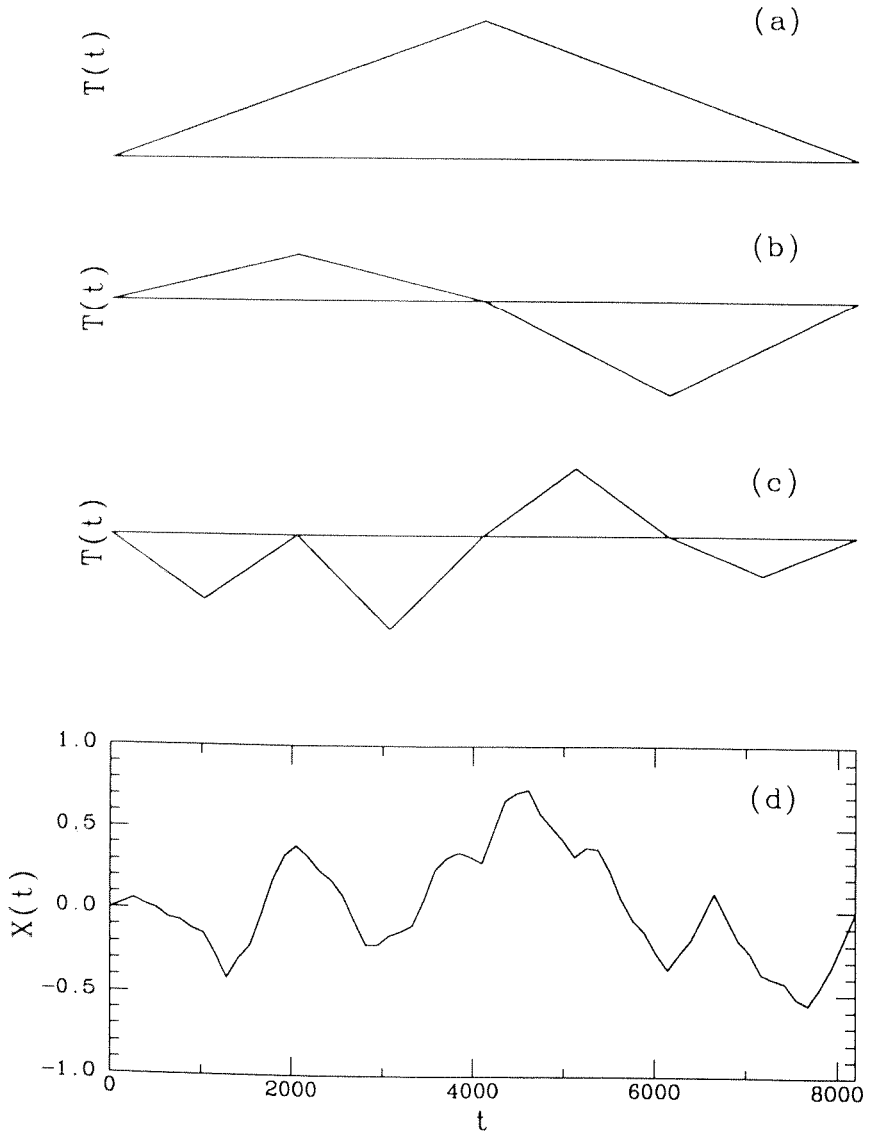

FIG 2

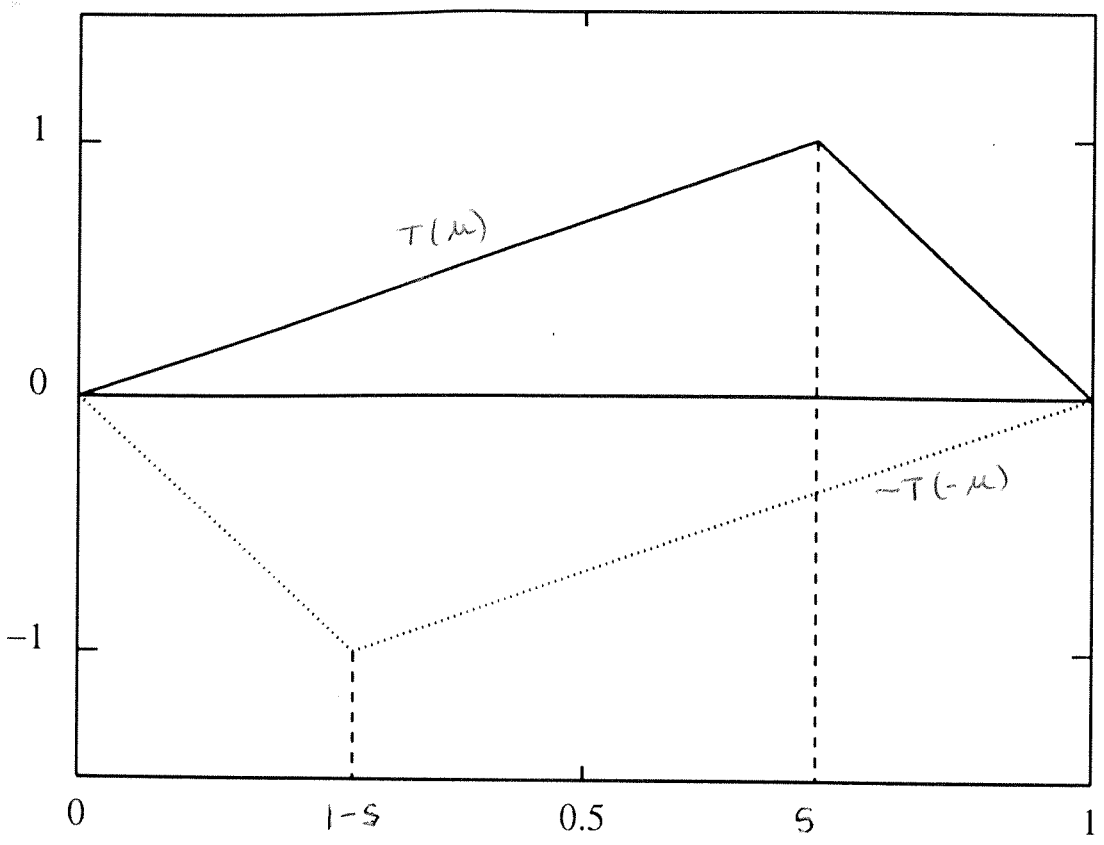

Fig 3

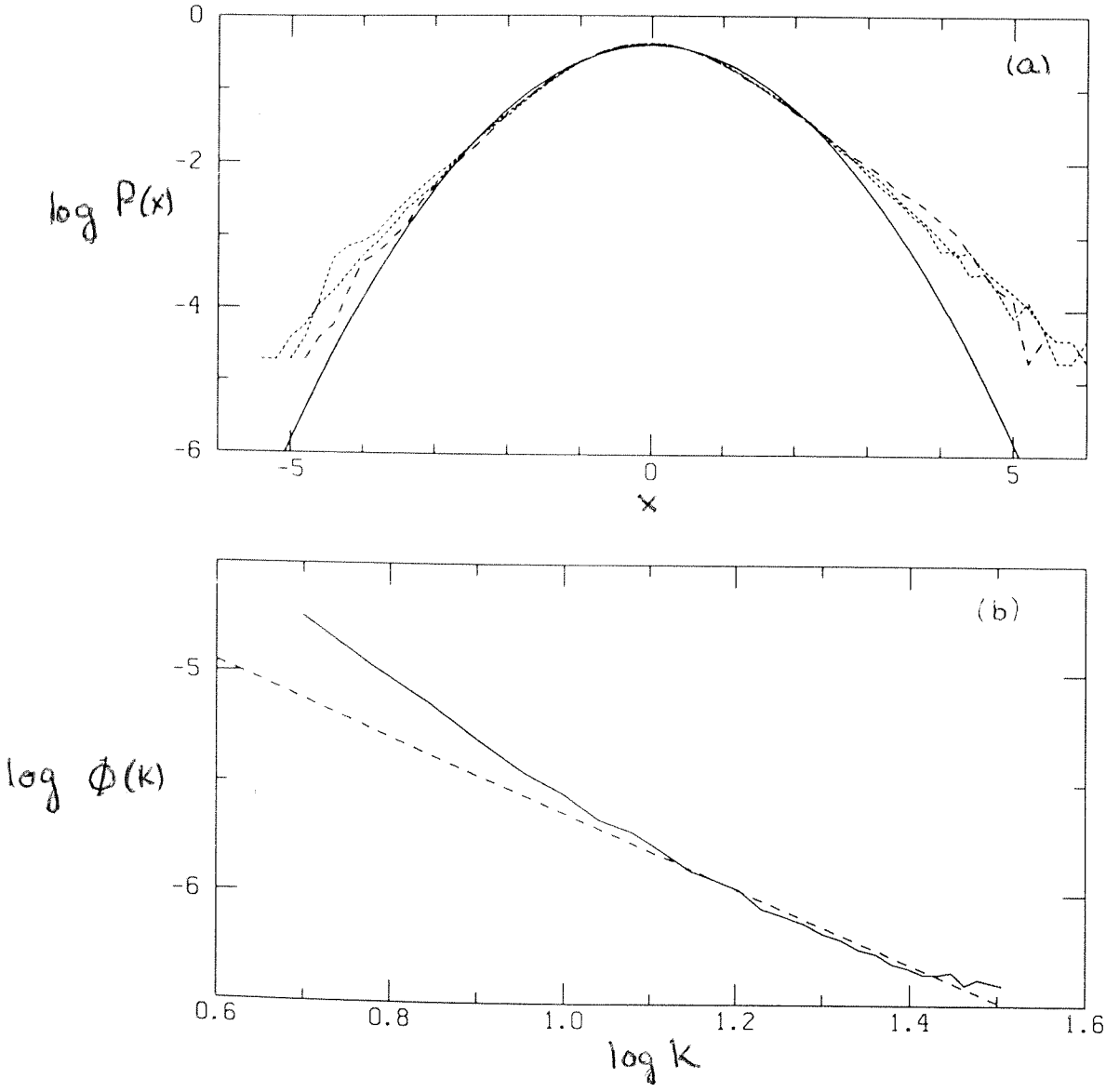

FIG 4

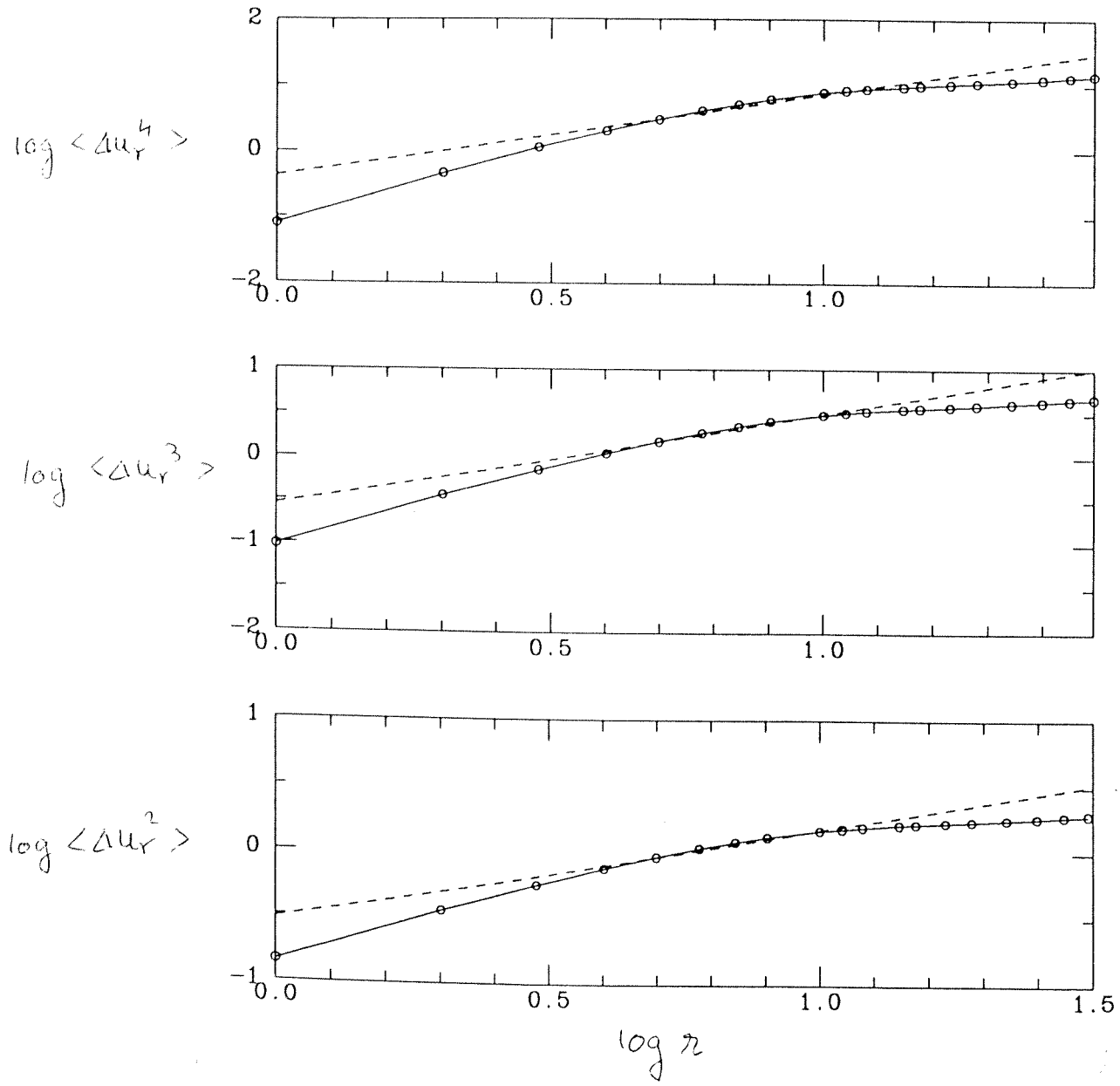
log $\langle \Delta u_r^4 \rangle$
log $\langle \Delta u_r^3 \rangle$
log $\langle \Delta u_r^2 \rangle$
2
0
−2
1
0
−1
−2
1
0
−1
0.0
0.5
1.0
0.0
0.5
1.0
0.0
0.5
1.0
1.5
log r

Fig. 5

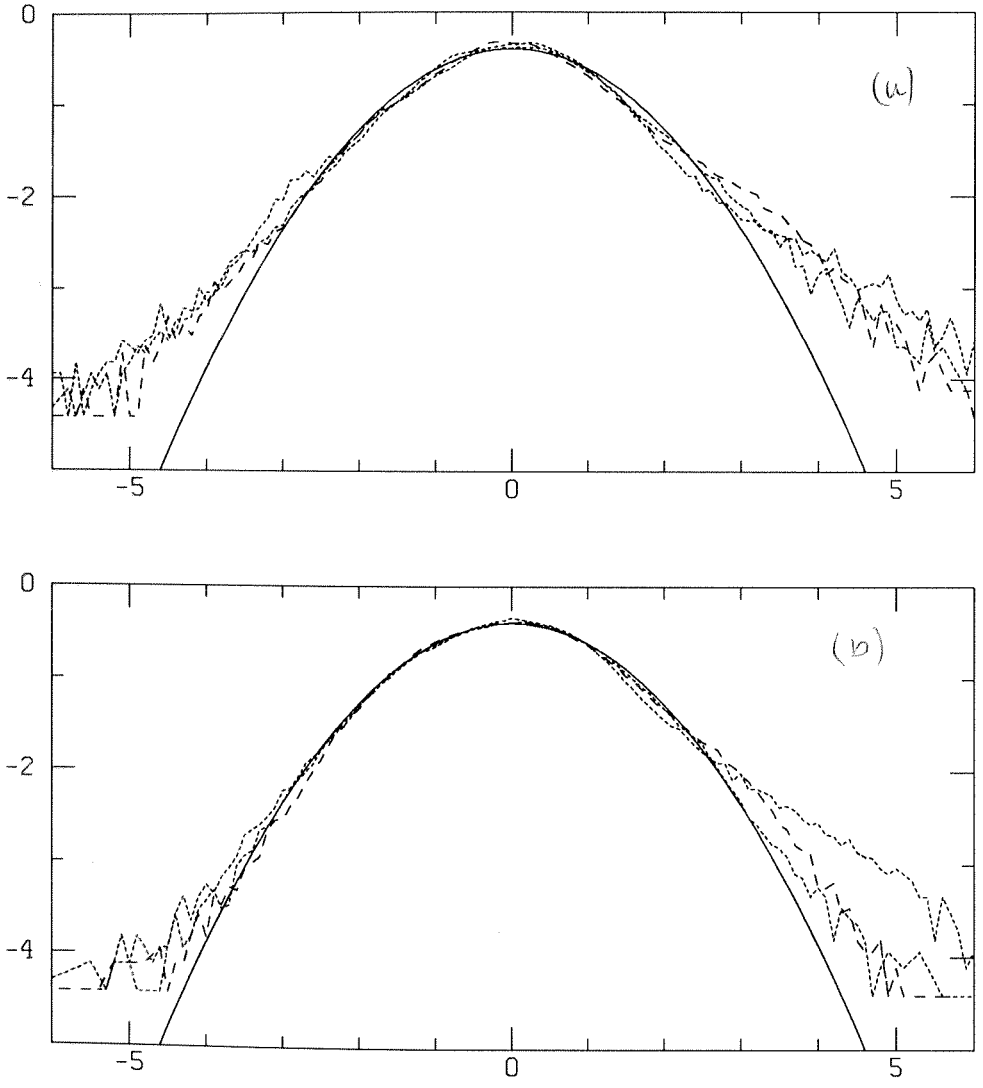

Fig 6

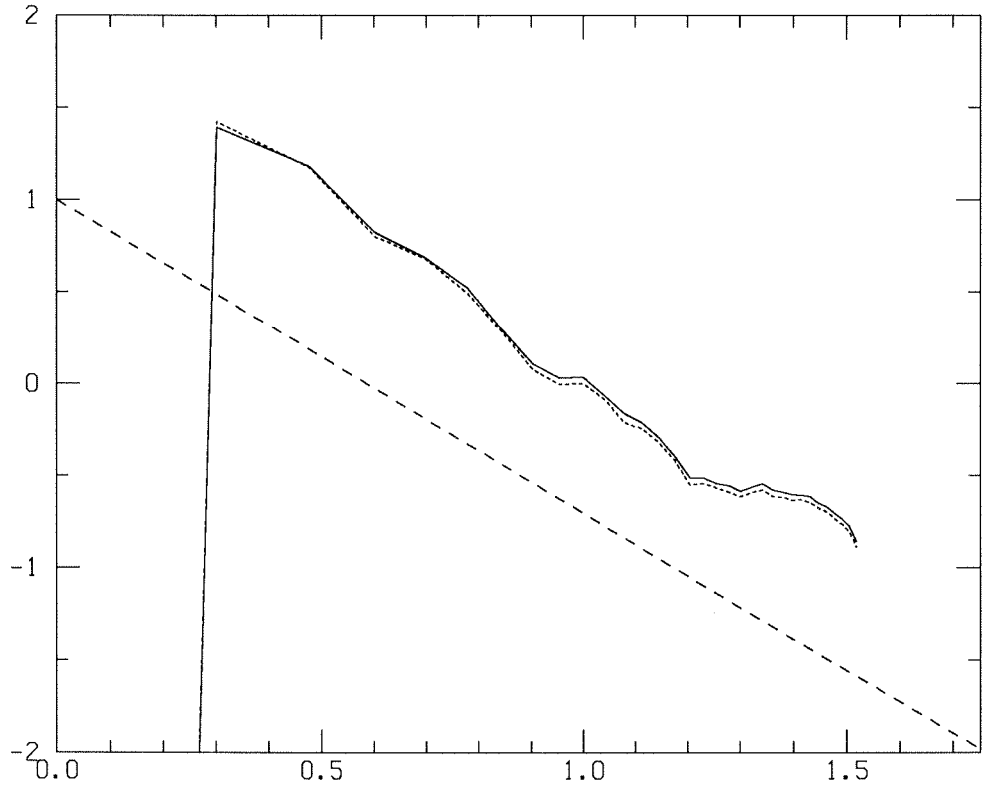

Fig 7

Before

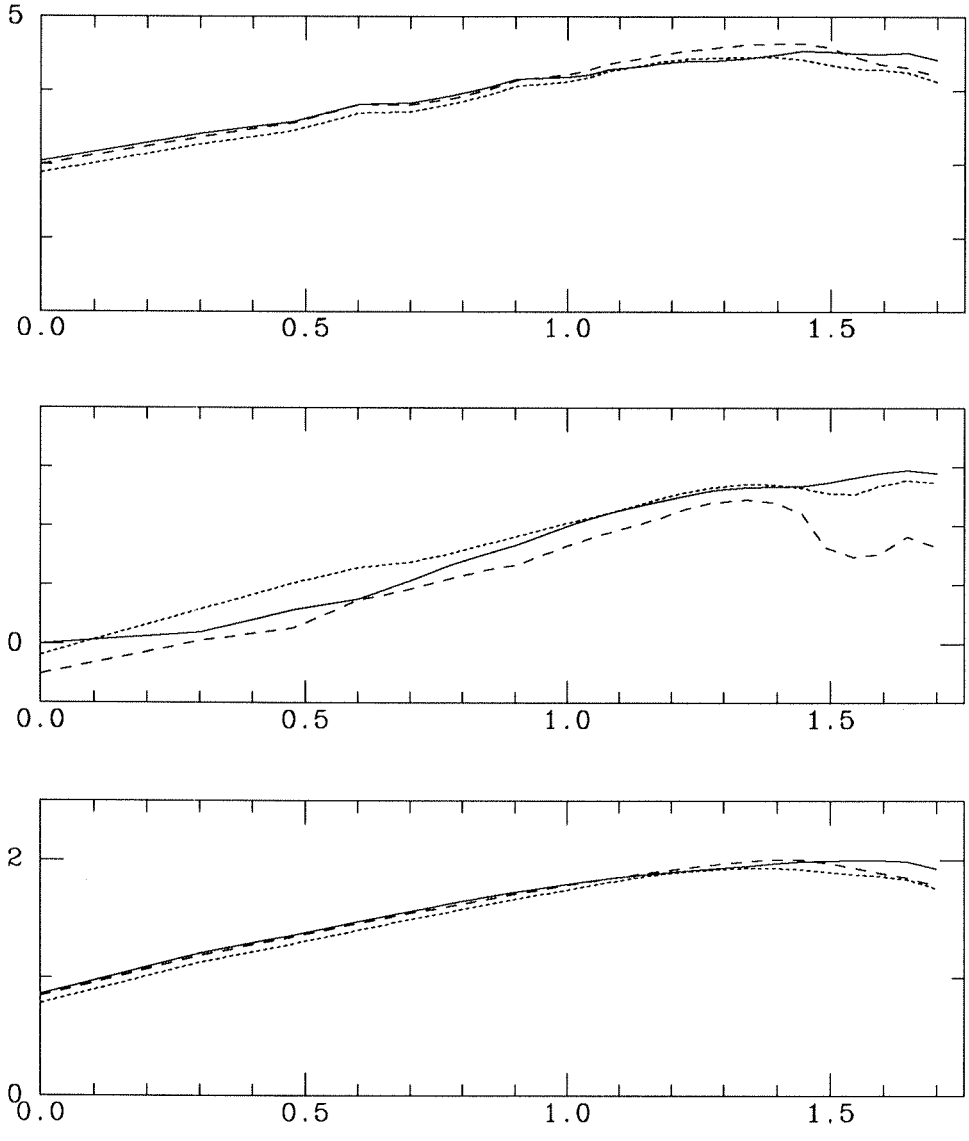

— u
- - - v
..... w

Fig 8 (a) Longitudinal Structure functions

After

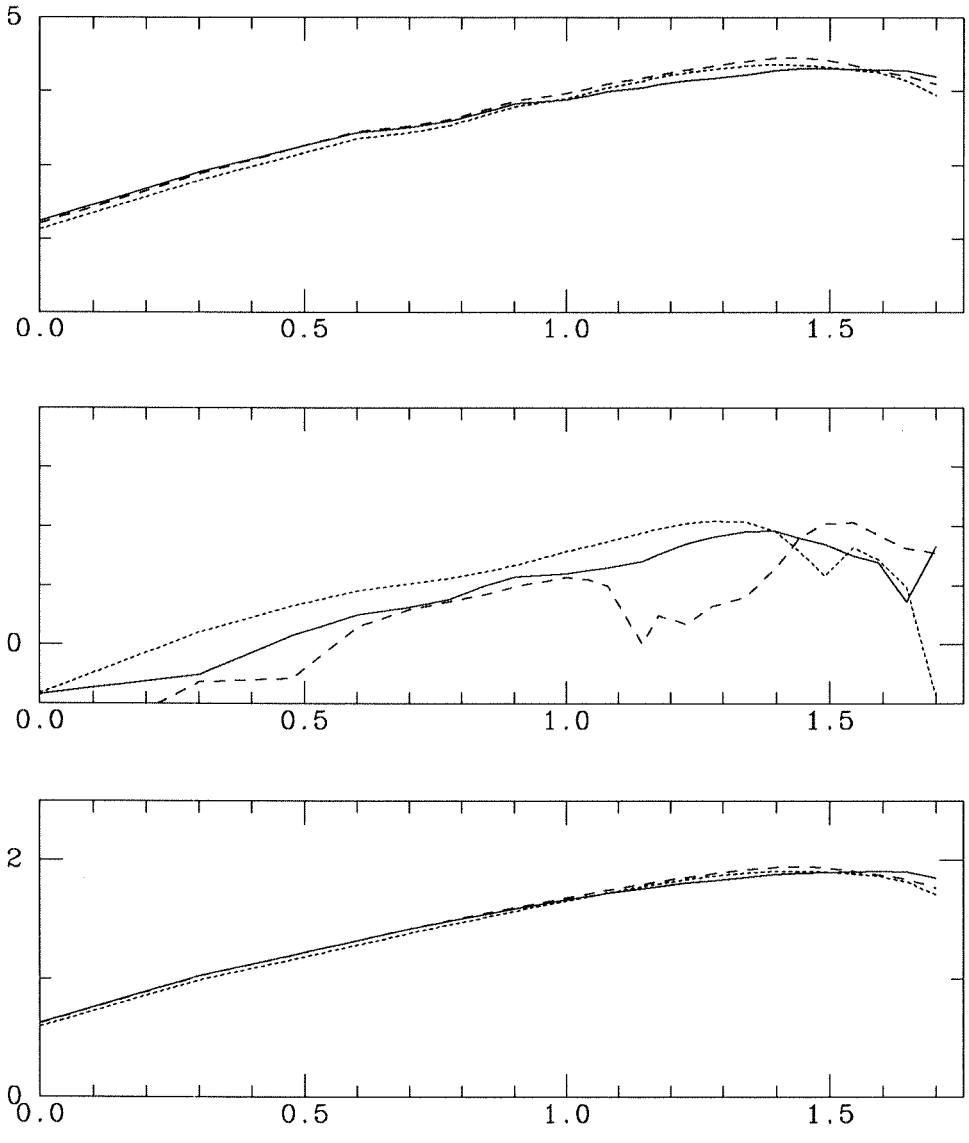

— u
--- v
..... w

FIG 8(b) Longitudinal Structure Functions

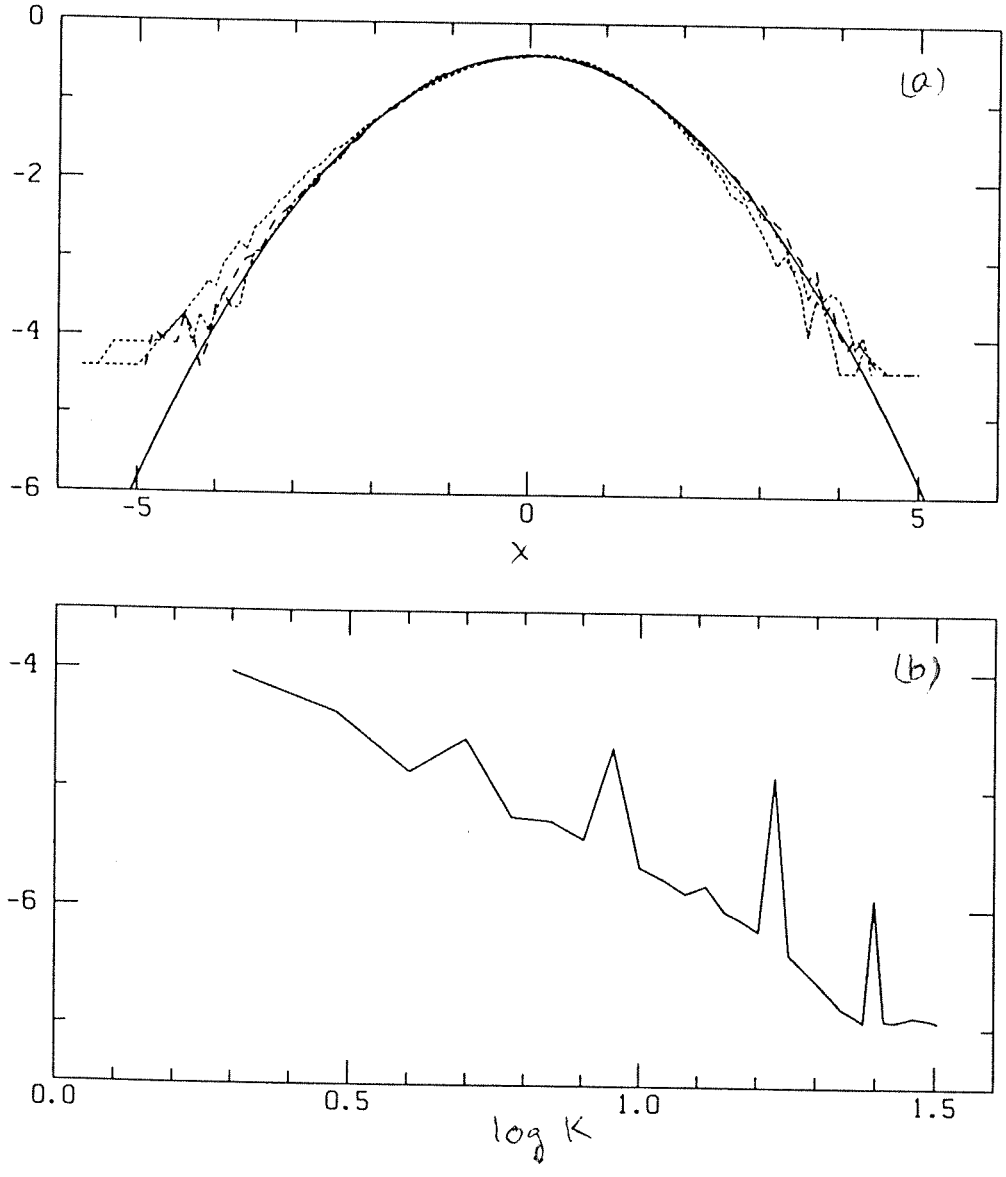

Fig 9

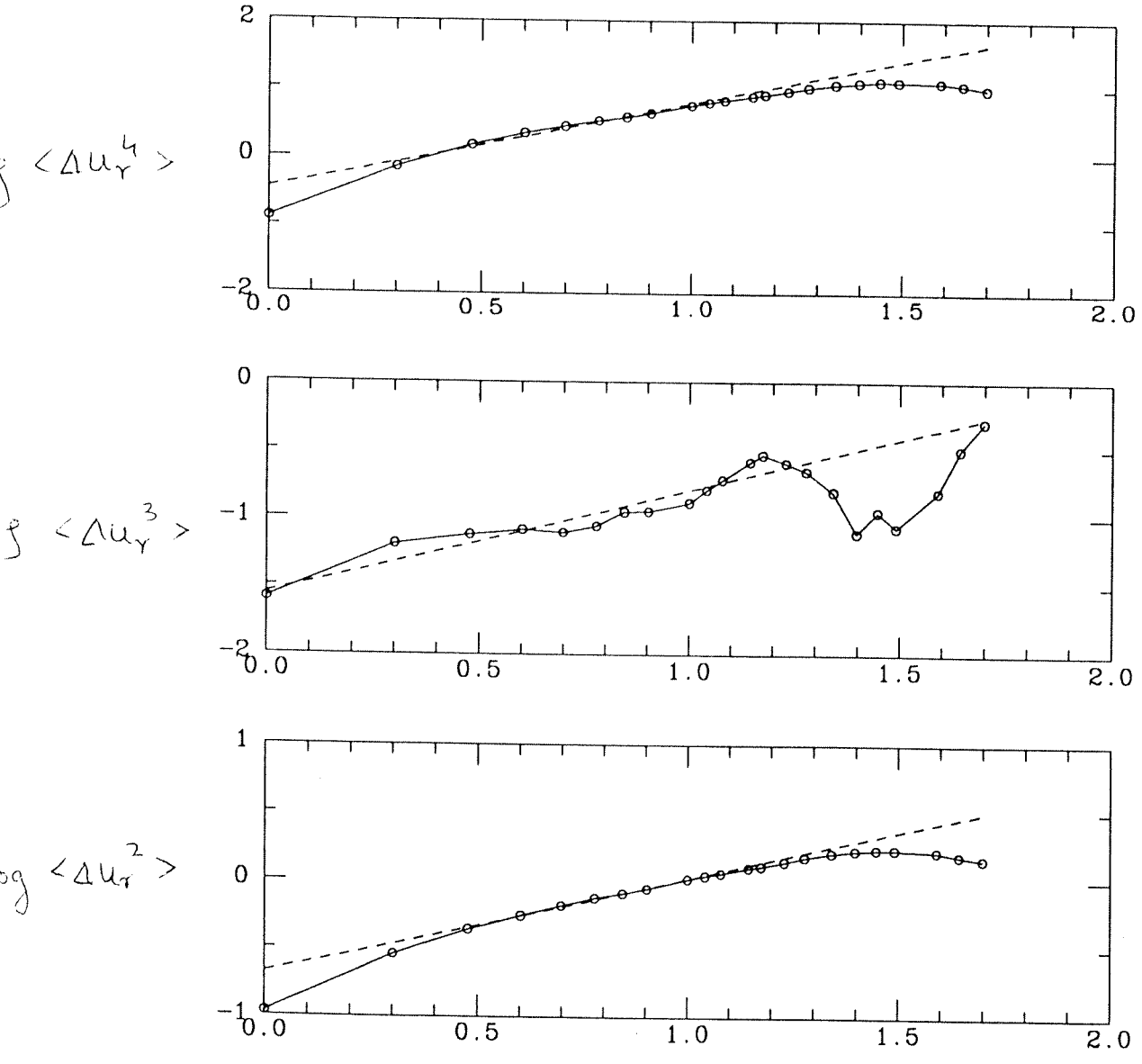

Fig 10

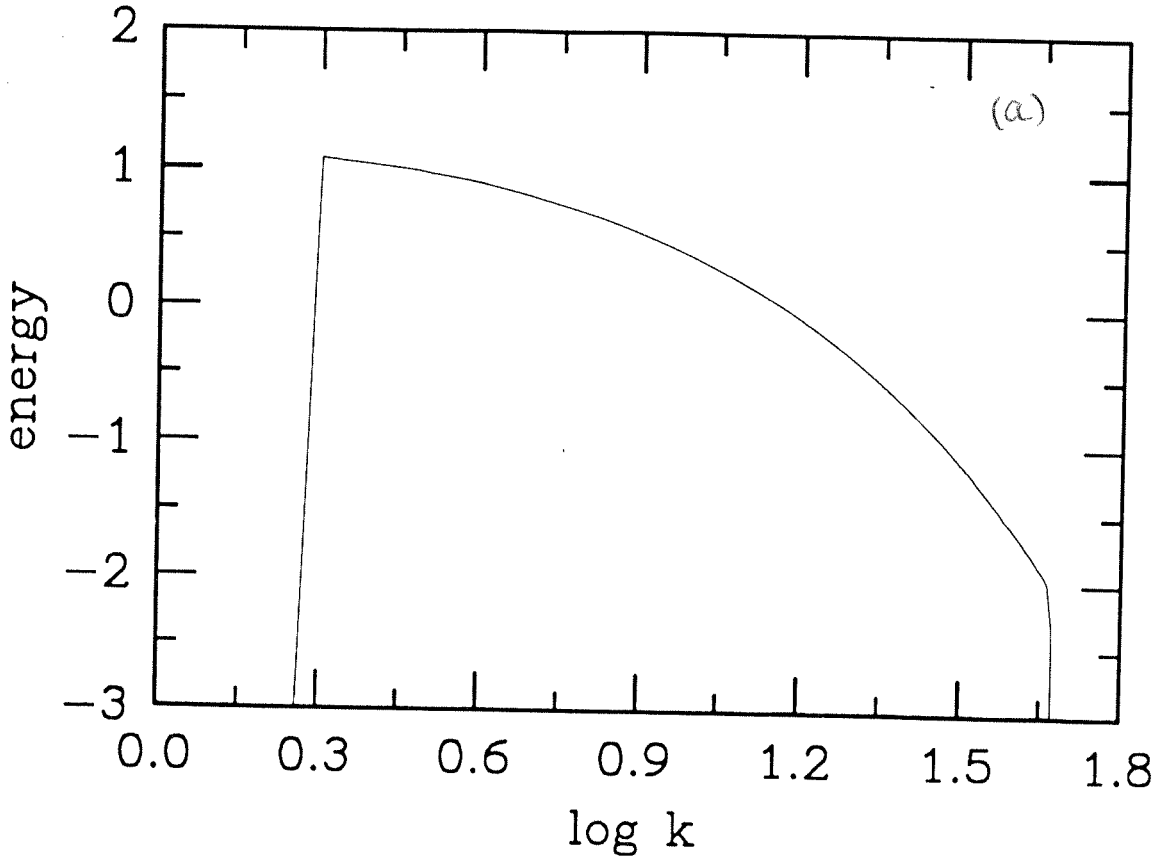
(a)
energy
2
1
0
−1
−2
−3
0.0
0.3
0.6
0.9
1.2
1.5
1.8
log k

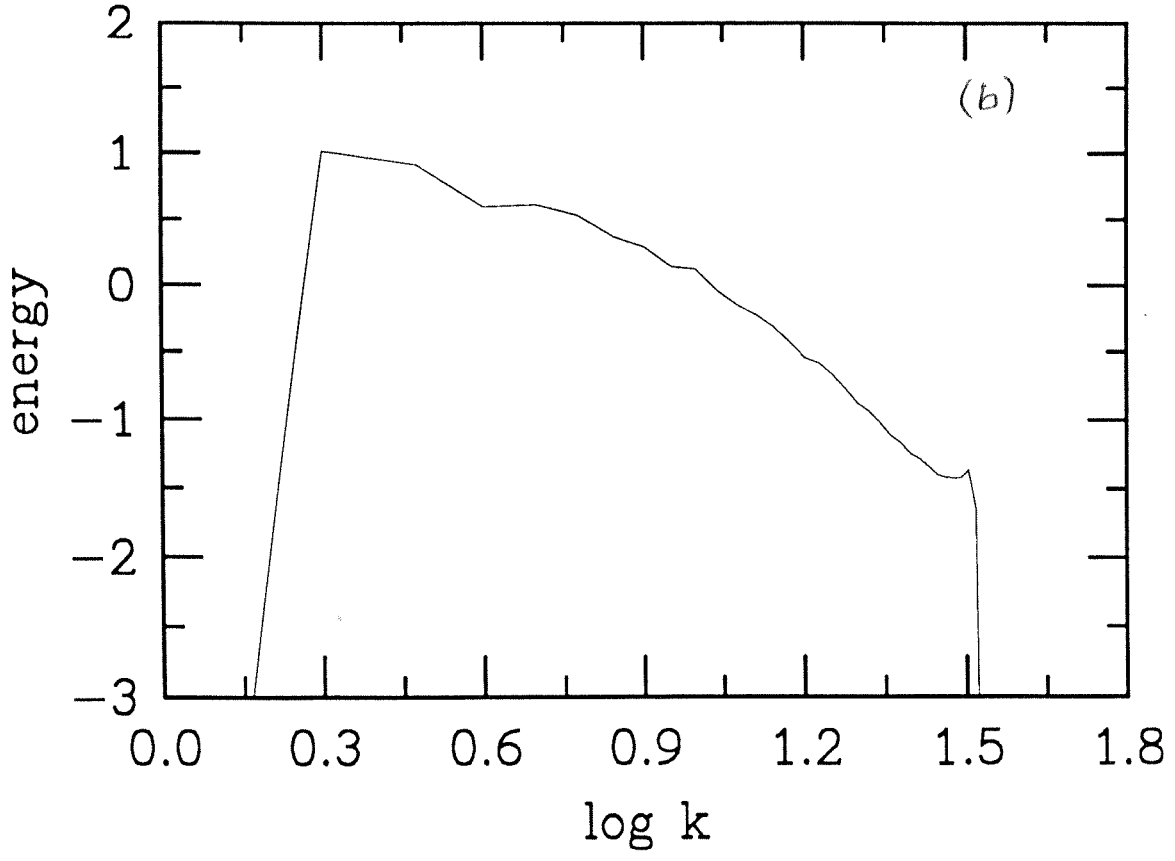
(b)
energy
2
1
0
−1
−2
−3
0.0
0.3
0.6
0.9
1.2
1.5
1.8
log k

Fig. 8\

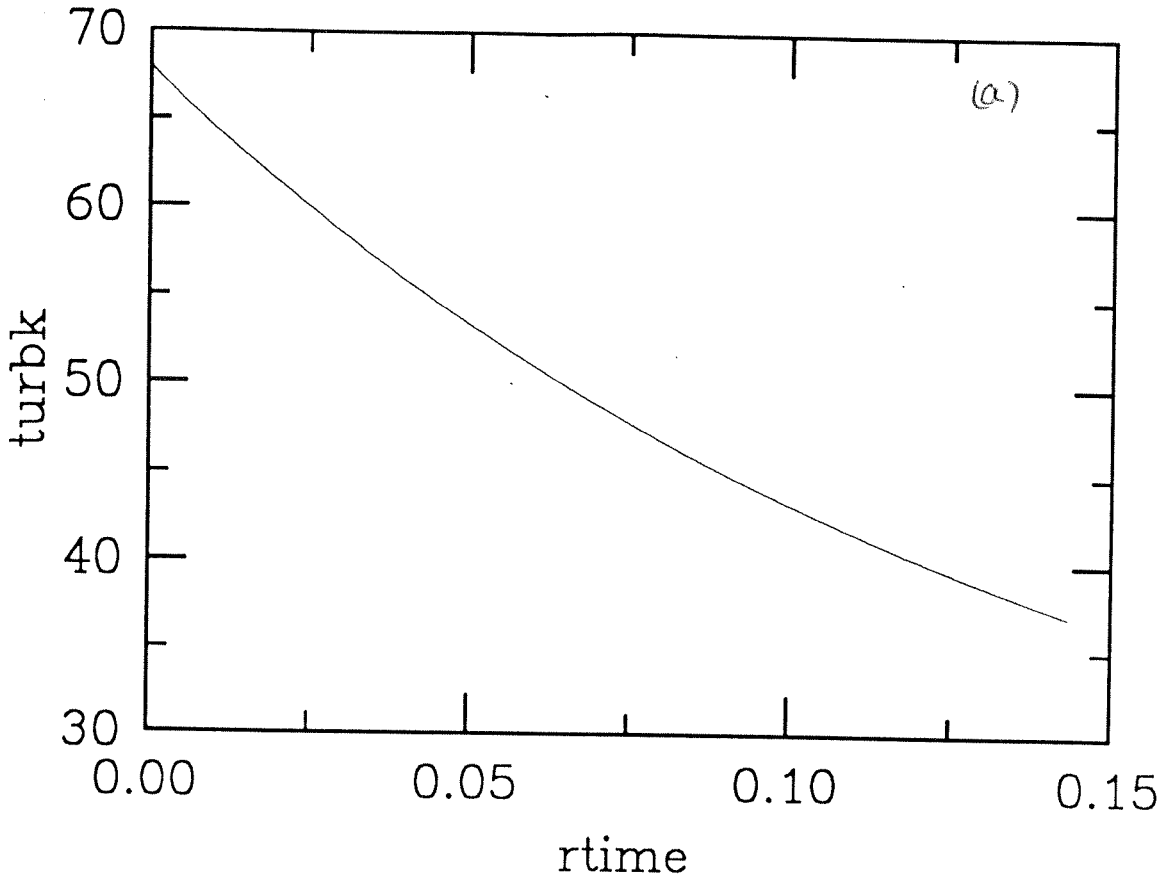
70
60
50
40
30
turbk
(a)
0.00
0.05
0.10
0.15
rtime

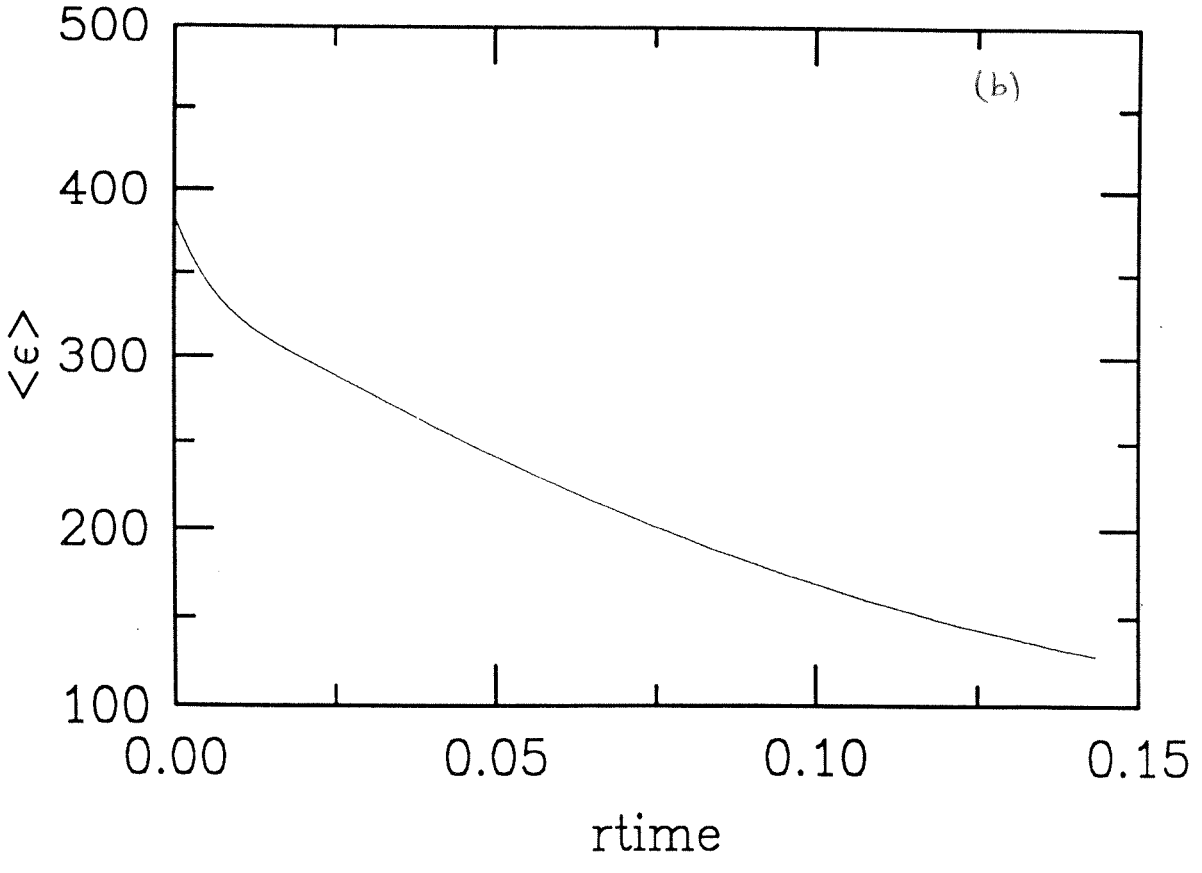
500
400
300
200
100
<ϵ>
(b)
0.00
0.05
0.10
0.15
rtime

FIG. 12

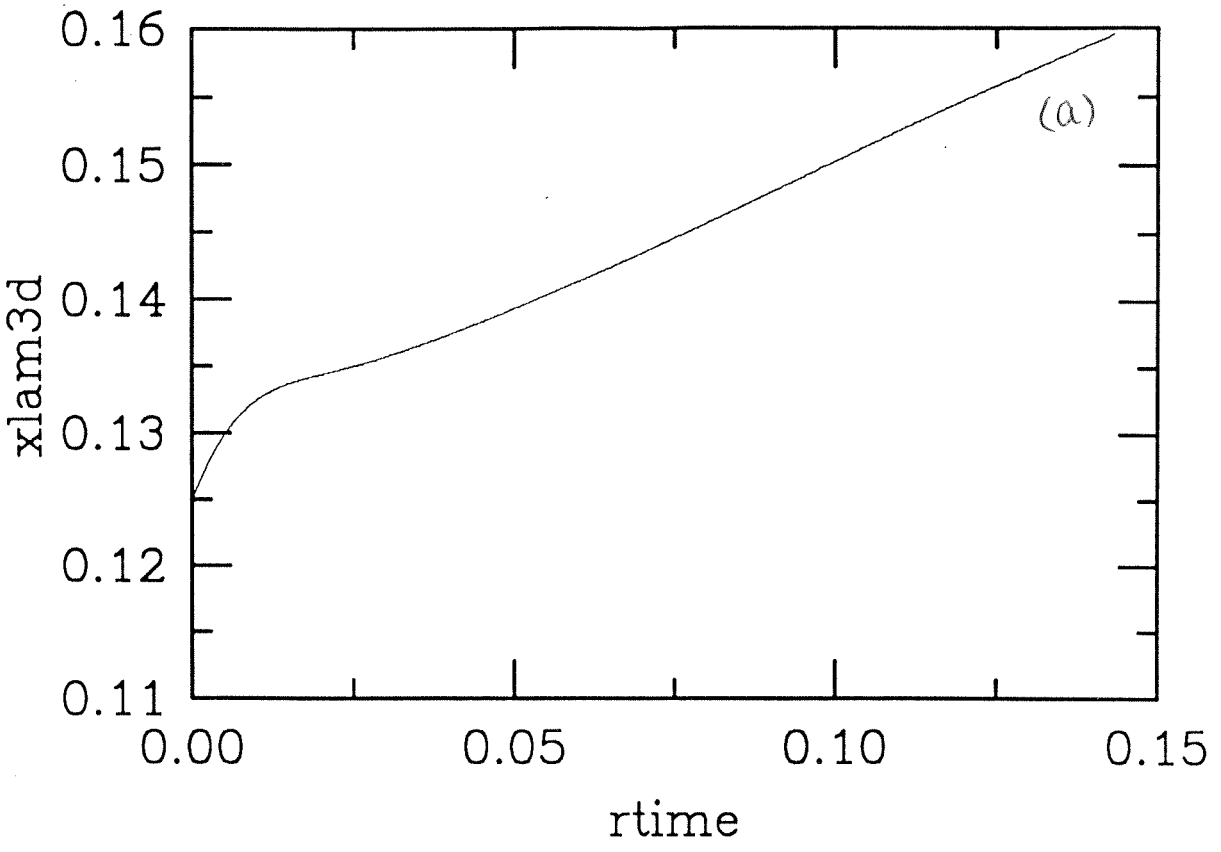
0.16
0.15
0.14
0.13
0.12
0.11
xlam3d
0.00
0.05
0.10
0.15
rtime
(a)

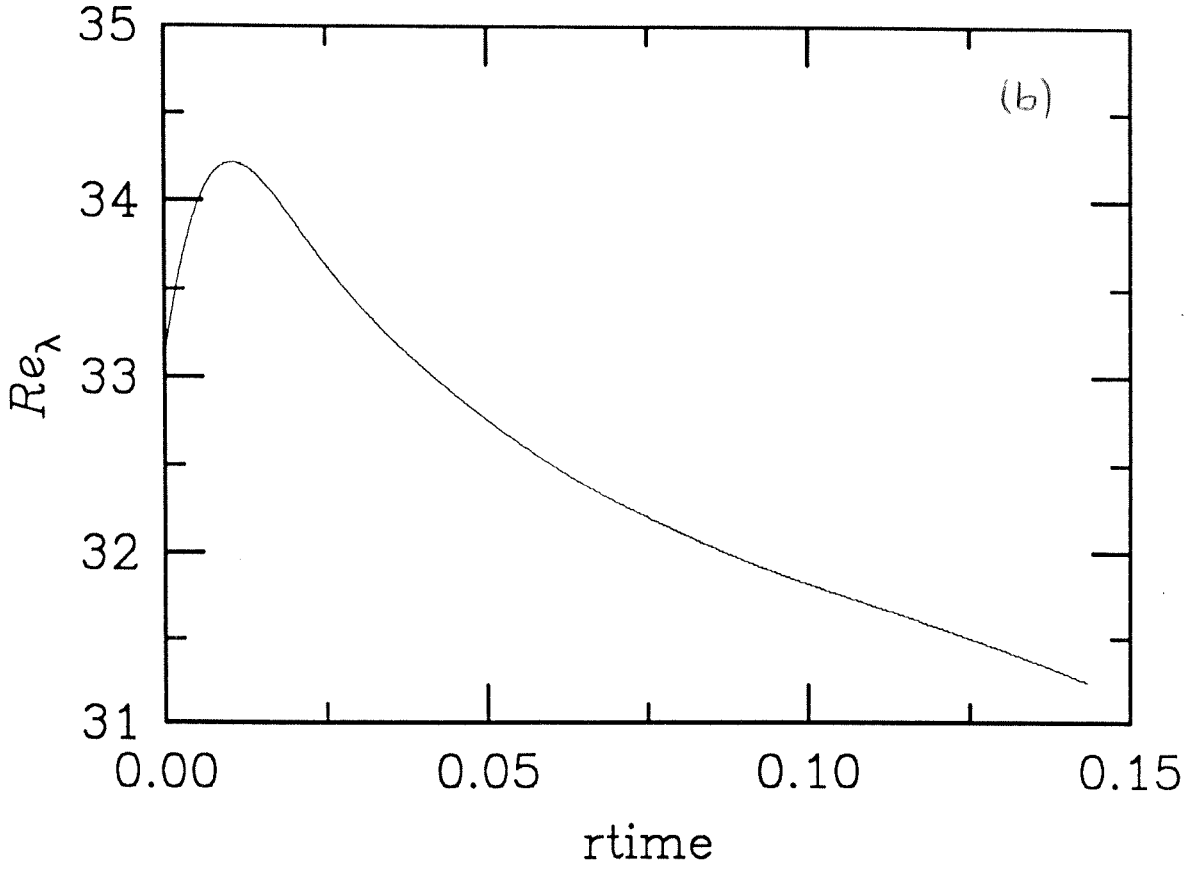
35
34
33
32
31
Re_λ
0.00
0.05
0.10
0.15
rtime
(b)

FIG. 13

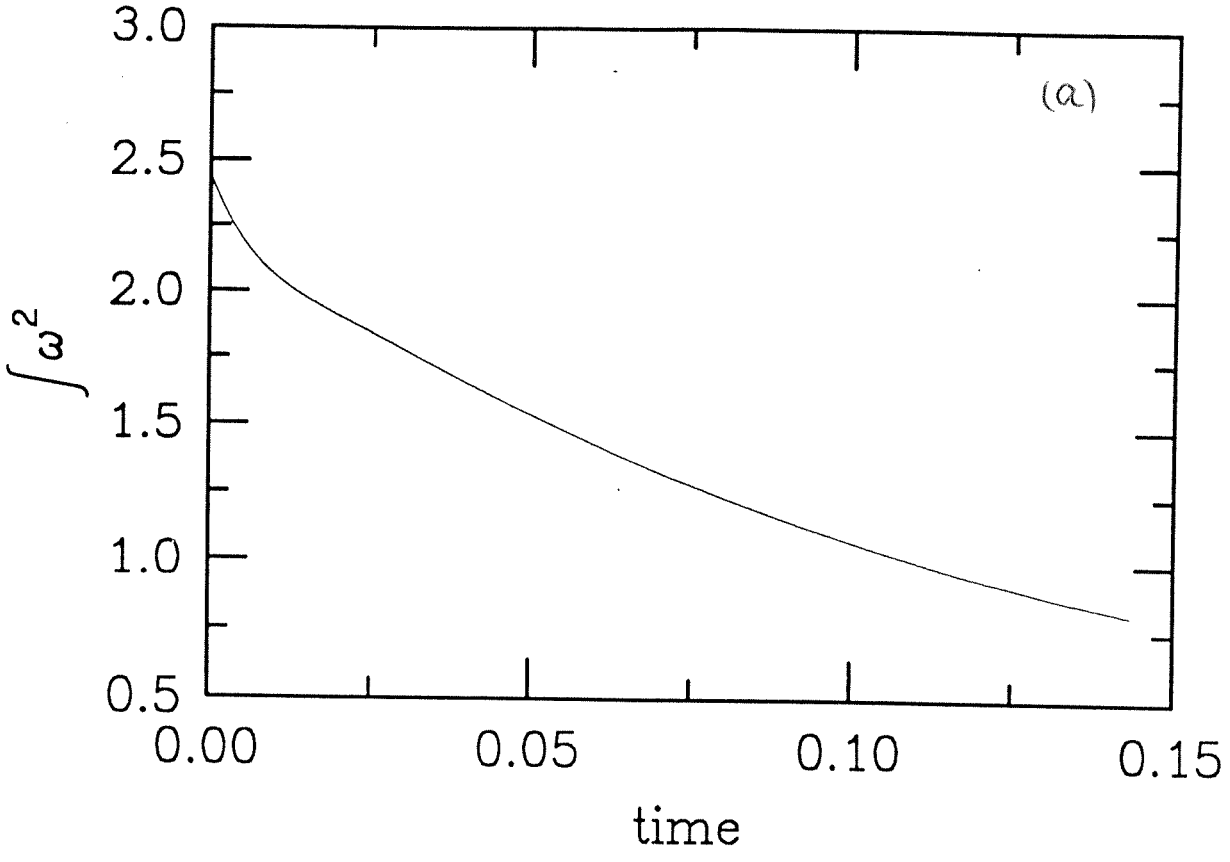
3.0
2.5
2.0
1.5
1.0
0.5
$\int \omega^2$
(a)
0.00
0.05
0.10
0.15
time

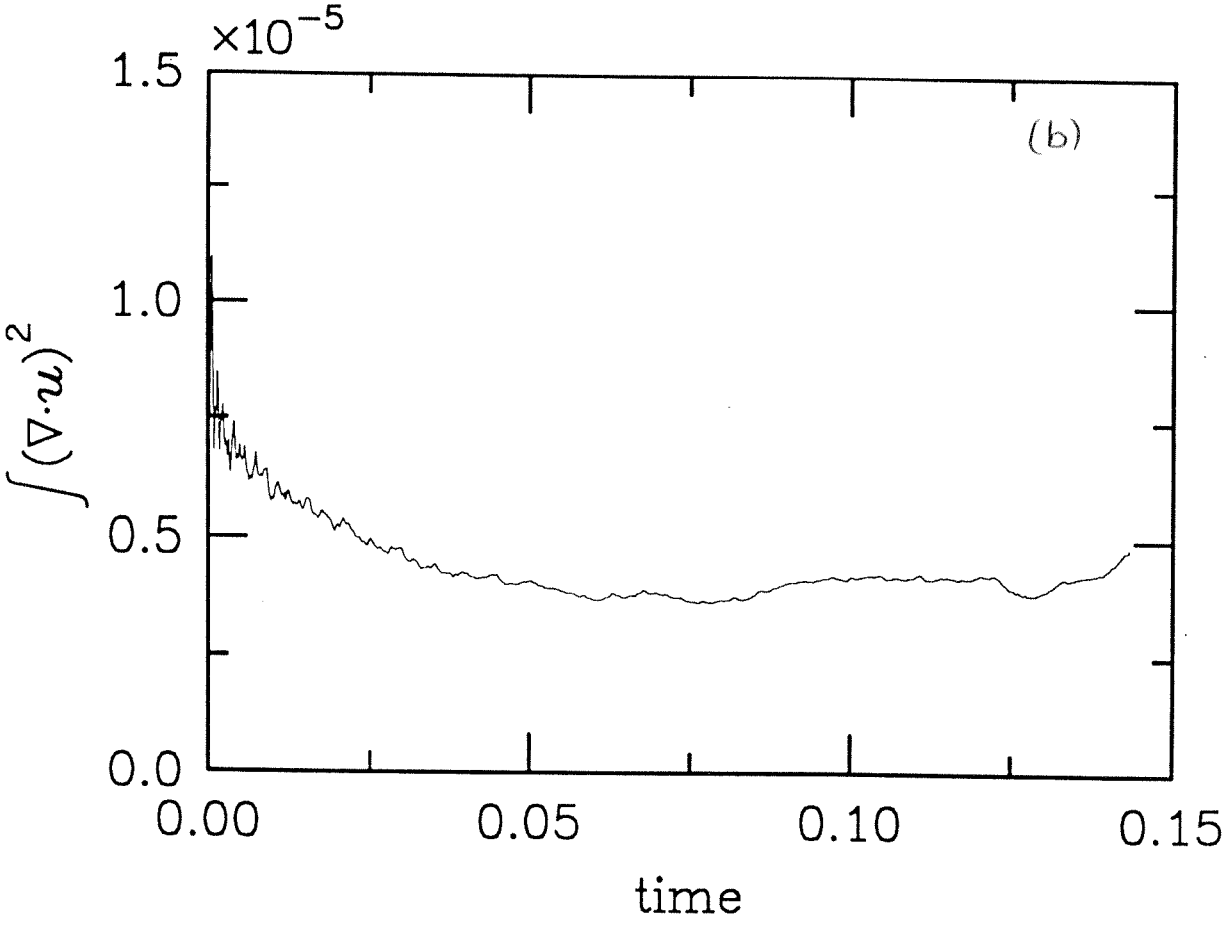
$\times 10^{-5}$
1.5
1.0
0.5
0.0
$\int (\nabla \cdot u)^2$
(b)
0.00
0.05
0.10
0.15
time

Fig. 14

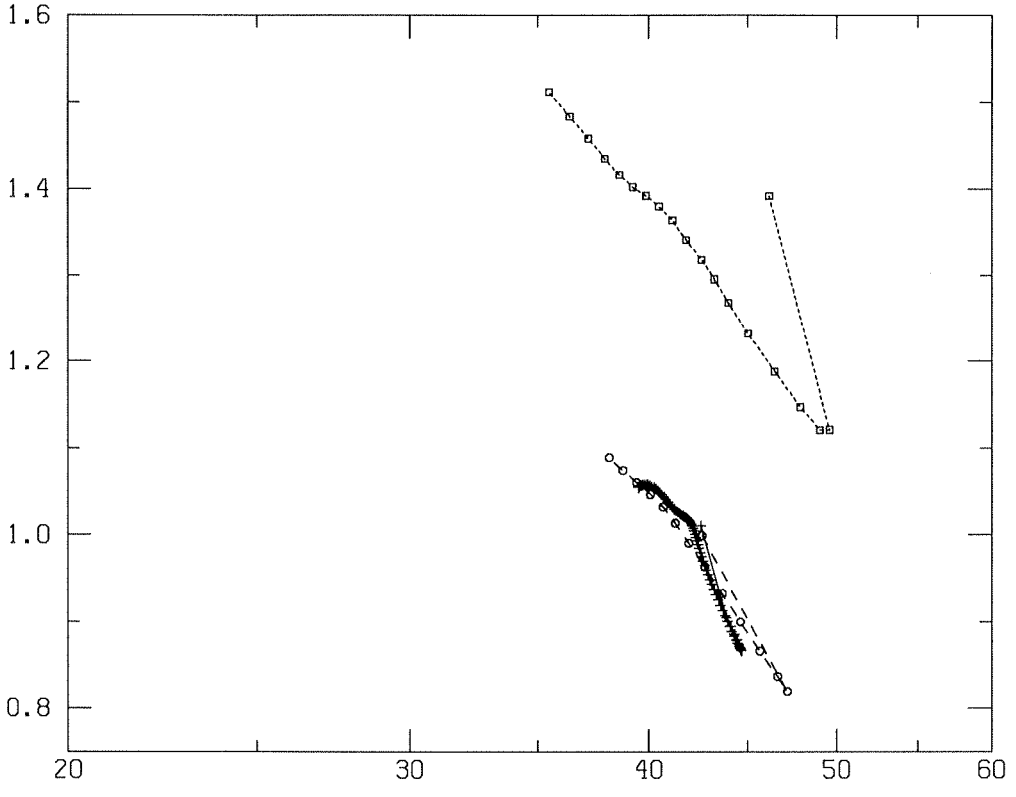
1.6
1.4
1.2
1.0
0.8
20
30
40
50
60
$\frac{\langle \varepsilon \rangle L}{u^3}$
R_λ

Fig 15

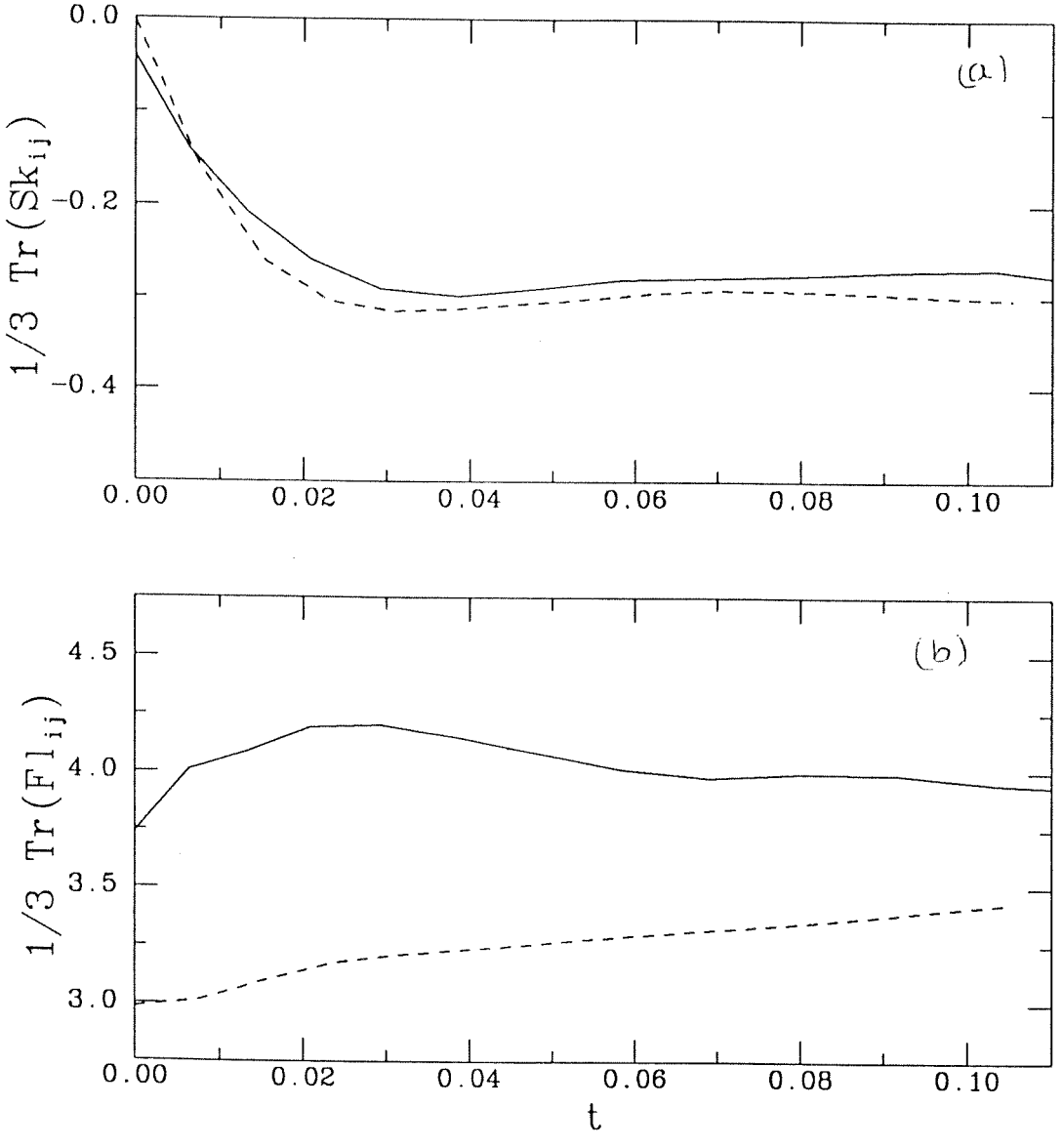
0.0
−0.2
−0.4
1/3 Tr(Sk$_{ij}$)
(a)
0.00
0.02
0.04
0.06
0.08
0.10
4.5
4.0
3.5
3.0
1/3 Tr(Fl$_{ij}$)
(b)
0.00
0.02
0.04
0.06
0.08
0.10
t

Fig 16

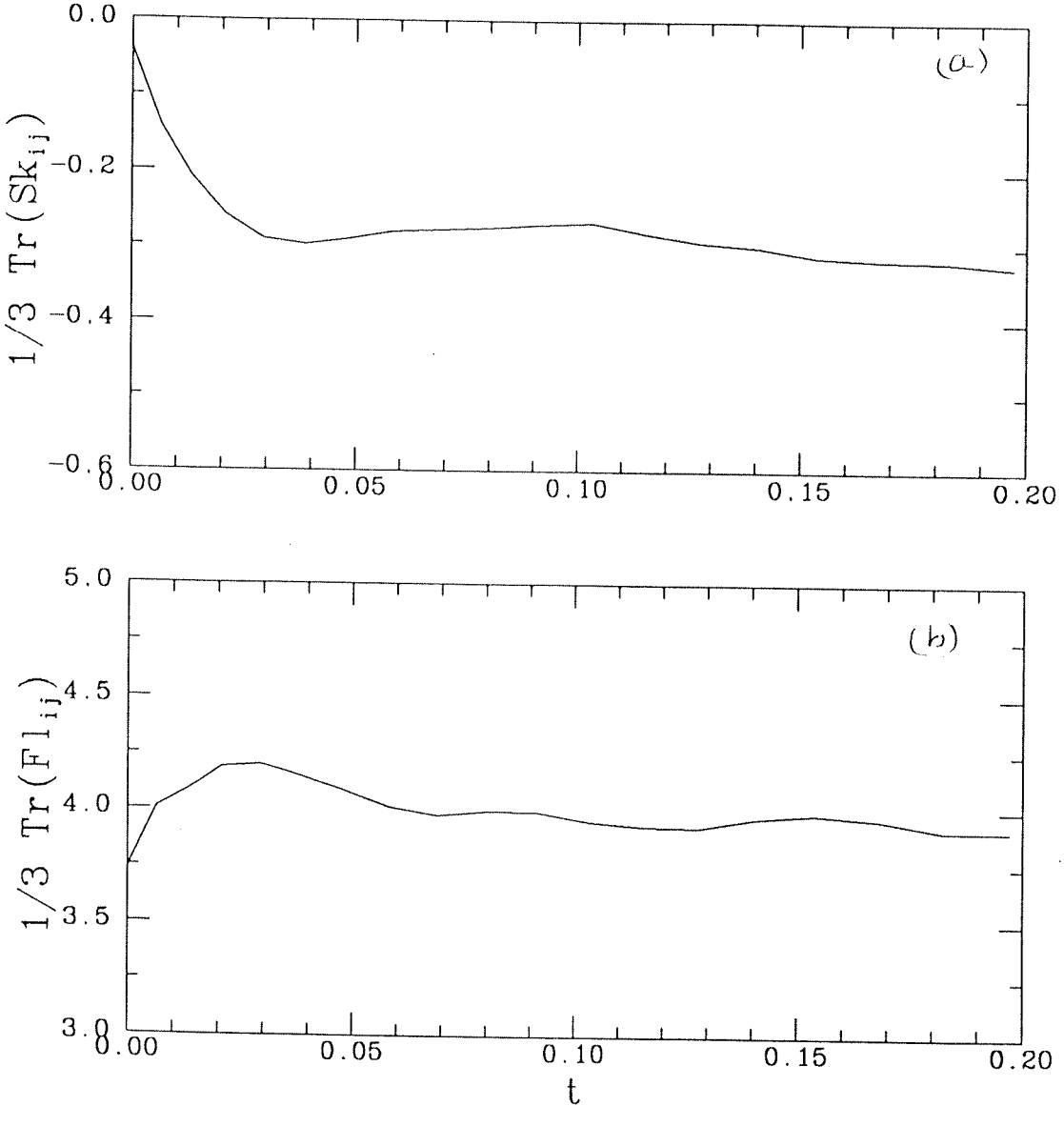
0.0
−0.2
−0.4
−0.6
1/3 Tr(Sk$_{ij}$)
(a)
0.00
0.05
0.10
0.15
0.20
5.0
4.5
4.0
3.5
3.0
1/3 Tr(Fl$_{ij}$)
(b)
0.00
0.05
0.10
0.15
0.20
t

Fig 17

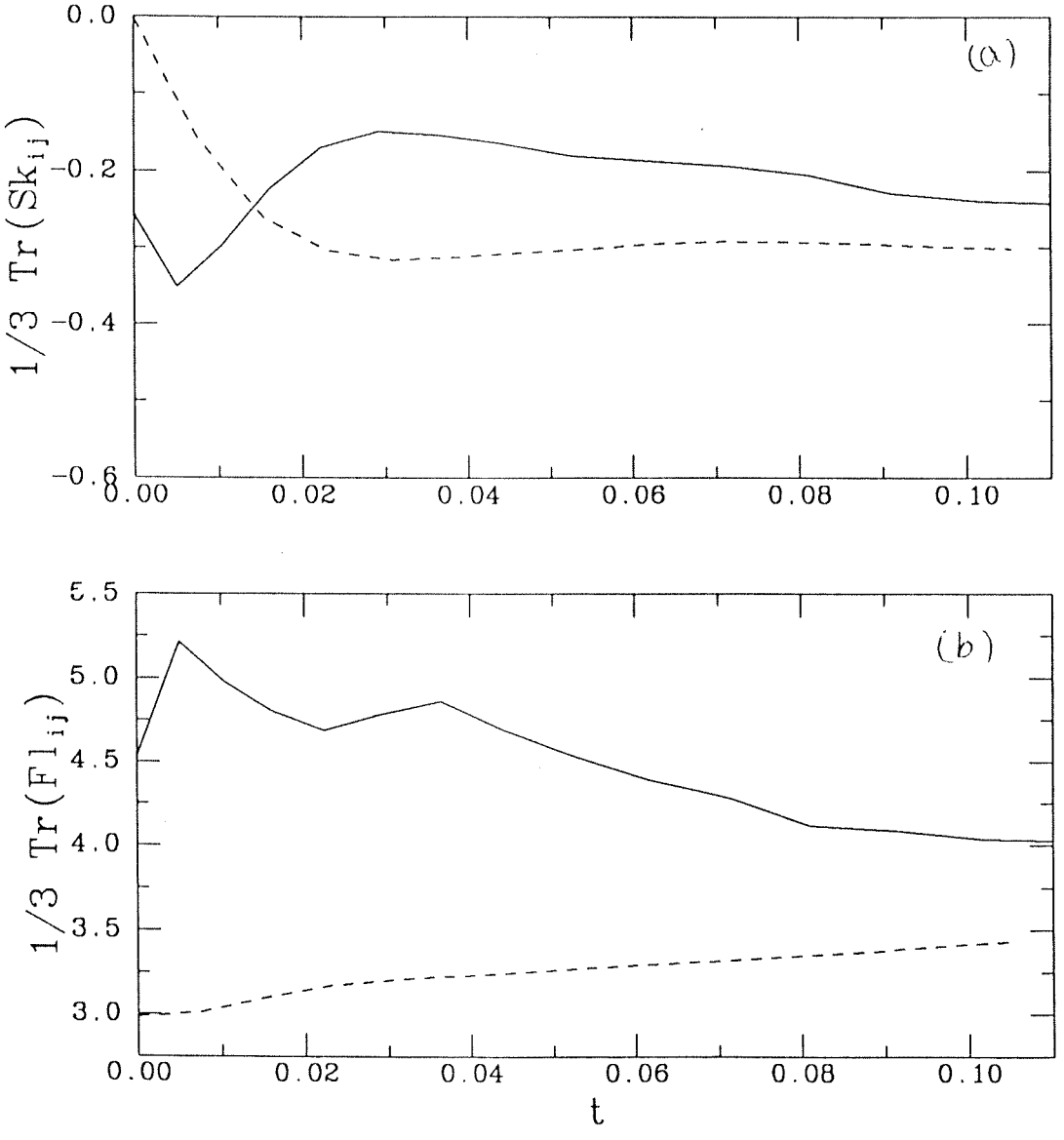
0.0
−0.2
−0.4
−0.6
1/3 Tr(Sk$_{ij}$)
(a)
0.00
0.02
0.04
0.06
0.08
0.10
5.5
5.0
4.5
4.0
3.5
3.0
1/3 Tr(Fl$_{ij}$)
(b)
0.00
0.02
0.04
0.06
0.08
0.10
t

Fig 18

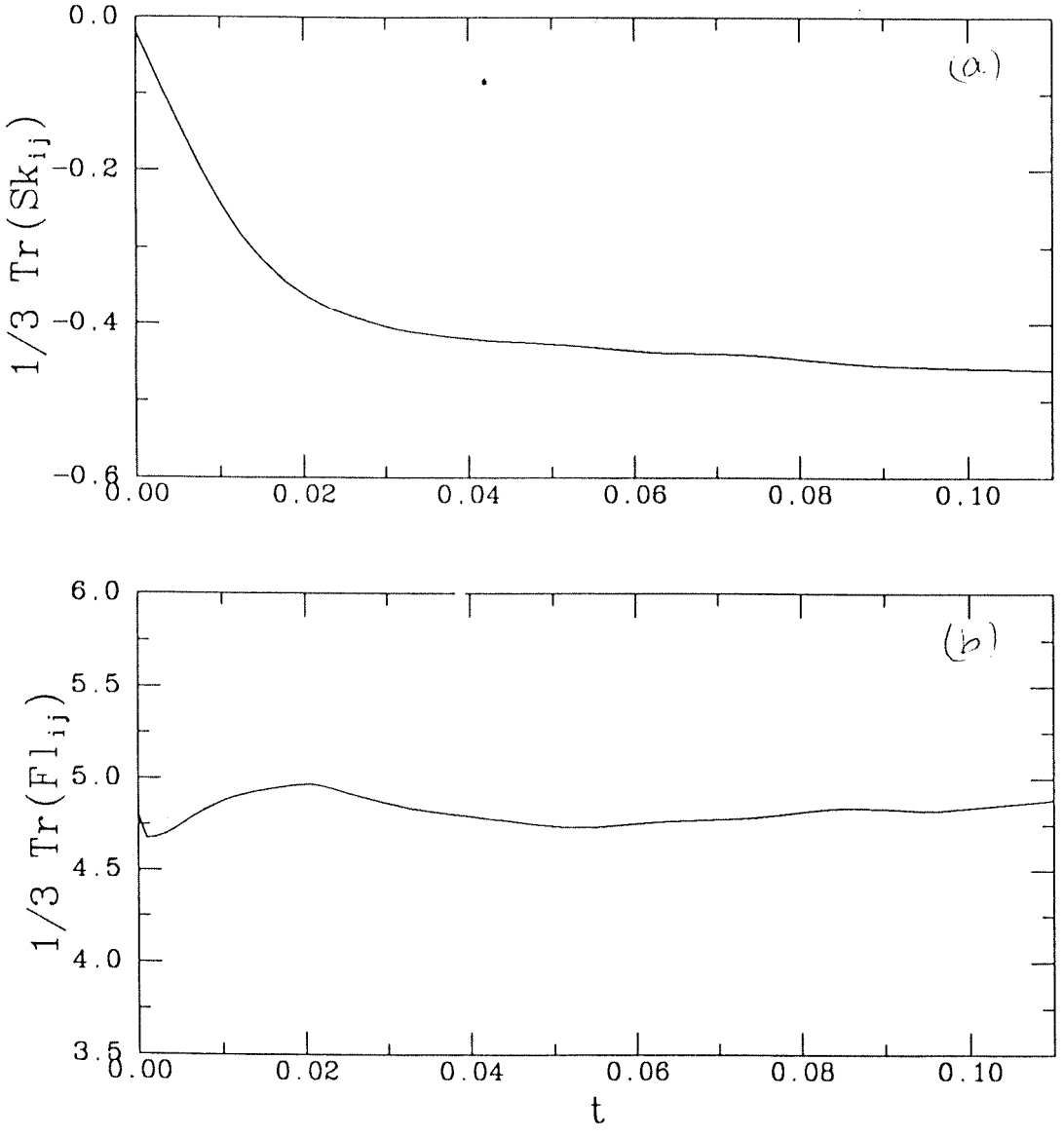
0.0
−0.2
−0.4
−0.6
1/3 Tr(Sk$_{ij}$)
(a)
0.00
0.02
0.04
0.06
0.08
0.10
6.0
5.5
5.0
4.5
4.0
3.5
1/3 Tr(Fl$_{ij}$)
(b)
t

Fig 19

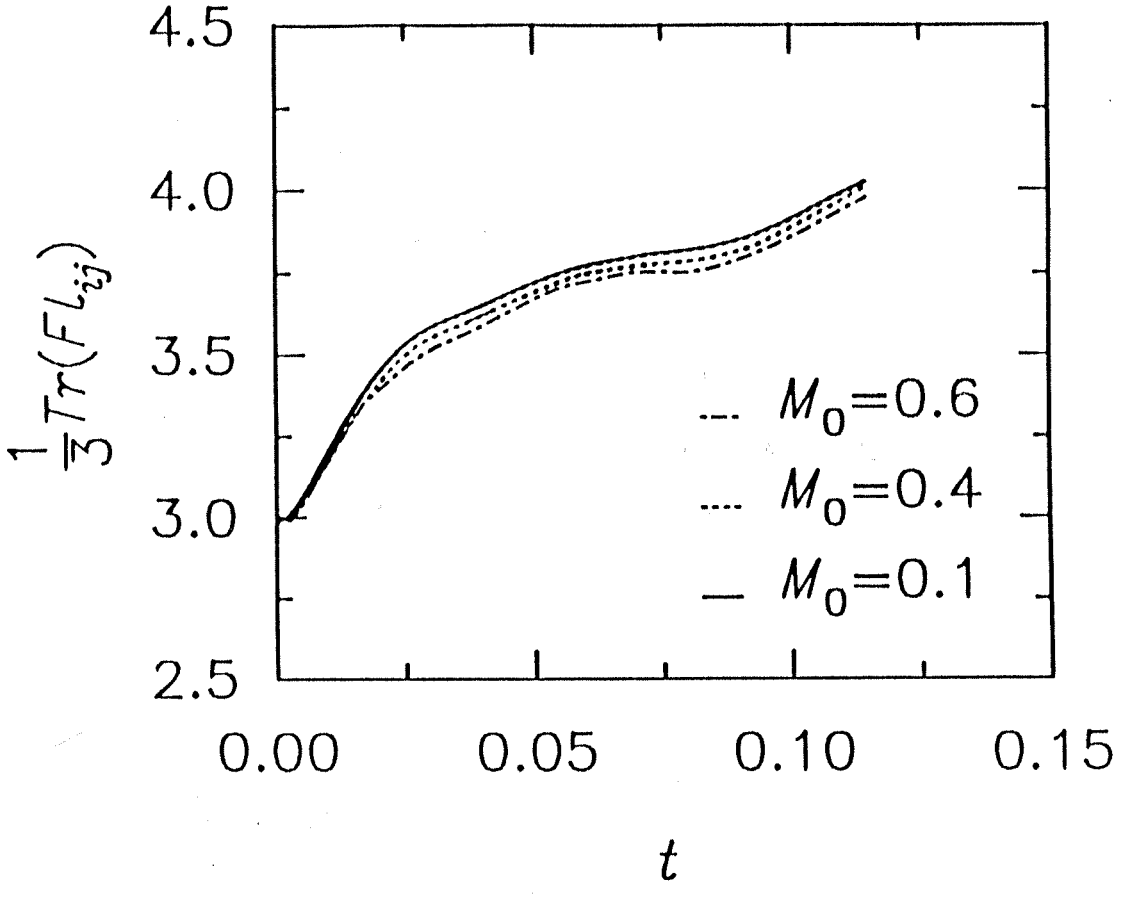

Fig. 6 Time history of one third the trace of Fl for M_0 of 0.0, 0.1, 0.4 and 0.6. Direct simulation was performed on a 96^3 grid. CBC initial conditions.

FIG. 20